CAMS Service Evolution

D4.5 Uncertainty in deposition – ensemble approach

Due date of deliverable	30 September 2025
Submission date	30 September 2025
File Name	CAMEO-D4-5-V1.1
Work Package /Task	WP4 T4.2
Organisation Responsible of Deliverable	HYGEOS
Author name(s)	Samuel Remy
Revision number	V1.1
Status	Issued
Dissemination Level	Public

Funded by the European Union

The CAMEO project (grant agreement No 101082125) is funded by the European Union.
Views and opinions expressed are however those of the author(s) only and do not necessarily reflect those of the European Union or the Commission. Neither the European Union nor the granting authority can be held responsible for them.

1 Executive Summary

Deposition products in CAMS can be of interest to several communities and represent a high added value potential product. However, the representation of deposition by atmospheric composition forecasting systems is fraught with uncertainties. They arise from various causes: modelling errors originate from representing processes in a simplified manner, partially, or not at all, as not all chemical and physical processes occurring in the atmosphere are well known or described. Emissions from anthropogenic or biogenic sources are hard to estimate and can be another source of uncertainty. Finally, many atmospheric composition processes are largely influenced by meteorology: most reaction rates depend on temperature, gas-particle partitioning between gaseous species and secondary inorganic aerosols depend on temperature and relative humidity; emissions of sea-salt and desert dust aerosols depend primarily on wind speed, deposition depends on precipitation and wind speed. Uncertainties in atmospheric composition modelling thus also result from uncertainties of simulated meteorological fields. Deposition of aerosols and trace gases is maybe the simulated quantity most impacted by uncertainties, as it combines uncertainties of meteorological quantities, in particular precipitation for wet deposition, and wind for dry deposition, and of the simulated burden, vertical distribution and concentration of the deposited species.

Copernicus Atmosphere Monitoring Service (CAMS) products are subjected from all these sources of error and uncertainty. In this deliverable report, we apply an ensemble methodology, inspired by and built from the ECMWF meteorological ensemble, to estimate the uncertainties of a selection of global CAMS prototype deposition products, using a configuration close to that of the currently operational cycle 49R1. Random perturbations have been applied to different components of IFS-COMPO, the atmospheric composition modelling system applied to produce global CAMS forecasts, and its inputs. The uncertainties introduced in this way are then propagated in the perturbed air quality forecasts, and the ensemble approach allows to quantify the mean uncertainty of the simulated fields through the ensemble spread. The resulting uncertainties are presented in this report for a selection of deposition products, periods and forecast times. They also provide a measure of how sensitive CAMS products are to errors from different causes (meteorology, emissions, modelling errors). These values should be used with care: the presented uncertainties depend on a lot of assumptions made about the original uncertainties. For the temporal uncertainties of emissions, input from work package 5 was used; for meteorology, we rely on the existing perturbation framework of the ECMWF meteorological ensemble, while for modelling uncertainties, a set of assumptions were made. Also, the uncertainties presented here are for 2021; however, it was shown that the uncertainties of CAMS products depend a lot on the meteorological and atmospheric composition of the day, which limits the validity and usefulness of monthly values.

For a realistic assessment of uncertainties, a well-balanced ensemble is needed. Well-balanced in this case means an ensemble that is able to capture the observed variability while not producing forecasts that are outside the observational space (over dispersion). Several evaluation tools have been developed in order to produce metrics to show how well-balanced the ensemble is. Those metrics are commonly used and presented for meteorological ensembles; however, their use in atmospheric composition is quite new. We'll present in detail these tools and how they were used. Most of the ensemblist diagnostics points to an under-dispersion or too small spread of the ensemble simulations that have been performed.

The propagation and relative importance of the different sources of uncertainty vary a lot depending on the species considered and the forecast time. In general, anthropogenic emissions were found to have a relatively smaller impact on the uncertainty of deposition products than other factors. For all parameters, meteorological and model uncertainties are the highest source of uncertainty. For the assessed species, dry deposition is less uncertain than wet deposition, very likely because its key meteorological input, wind speed, is less subject to uncertainties than the precipitation fluxes that modulate simulated wet deposition.

Table of Contents

2 Introduction

2.1 Background

Monitoring the composition of the atmosphere is a key objective of the European Union's flagship Space programme Copernicus, with the Copernicus Atmosphere Monitoring Service (CAMS) providing free and continuous data and information on atmospheric composition.

The CAMS Service Evolution (CAMEO) project will enhance the quality and efficiency of the CAMS service and help CAMS to better respond to policy needs such as air pollution and greenhouse gases monitoring, the fulfilment of sustainable development goals, and sustainable and clean energy.

CAMEO will help prepare CAMS for the uptake of forthcoming satellite data, including Sentinel-4, -5 and 3MI, and advance the aerosol and trace gas data assimilation methods and inversion capacity of the global and regional CAMS production systems.

CAMEO will develop methods to provide uncertainty information about CAMS products, in particular for emissions, policy, solar radiation and deposition products in response to prominent requests from current CAMS users.

CAMEO will contribute to the medium- to long-term evolution of the CAMS production systems and products.

The transfer of developments from CAMEO into subsequent improvements of CAMS operational service elements is a main driver for the project and is the main pathway to impact for CAMEO.

The CAMEO consortium, led by ECMWF, the entity entrusted to operate CAMS, includes several CAMS partners thus allowing CAMEO developments to be carried out directly within the CAMS production systems and facilitating the transition of CAMEO results to future upgrades of the CAMS service.

This will maximise the impact and outcomes of CAMEO as it can make full use of the existing CAMS infrastructure for data sharing, data delivery and communication, thus supporting policymakers, business and citizens with enhanced atmospheric environmental information.

2.2 Scope of this deliverable

2.2.1 Objectives of this deliverable

In this deliverable an atmospheric composition ensemble has been developed, evaluated and used to provide quantitative estimates of the uncertainties of CAMS deposition products.

2.2.2 Work performed in this deliverable

In this deliverable the work as planned in the Description of Action (DoA, WP4 T4.2) was performed.

2.2.3 Deviations and counter measures

No deviations have been encountered.

2.2.4 CAMEO Project Partners:

ECMWF	EUROPEAN CENTRE FOR MEDIUM-RANGE WEATHER FORECASTS
Met Norway	METEOROLOGISK INSTITUTT
BSC	BARCELONA SUPERCOMPUTING CENTER-CENTRO NACIONAL DE SUPERCOMPUTACION
KNMI	KONINKLIJK NEDERLANDS METEOROLOGISCH INSTITUUT-KNMi
SMHI	SVERIGES METEOROLOGISKA OCH HYDROLOGISKA INSTITUT
BIRA-IASB	INSTITUT ROYAL D'AERONOMIE SPATIALEDE BELGIQUE
HYGEOS	HYGEOS SARL
FMI	ILMATIETEEN LAITOS
DLR	DEUTSCHES ZENTRUM FUR LUFT - UND RAUMFAHRT EV
ARMINES	ASSOCIATION POUR LA RECHERCHE ET LE DEVELOPPEMENT DES METHODES ET PROCESSUS INDUSTRIELS
CNRS	CENTRE NATIONAL DE LA RECHERCHE SCIENTIFIQUE CNRS
GRASP-SAS	GENERALIZED RETRIEVAL OF ATMOSPHERE AND SURFACE PROPERTIES EN ABREGE GRASP
CU	UNIVERZITA KARLOVA
CEA	COMMISSARIAT A L ENERGIE ATOMIQUE ET AUX ENERGIES ALTERNATIVES
MF	METEO-FRANCE
TNO	NEDERLANDSE ORGANISATIE VOOR TOEGEPAST NATUURWETENSCHAPPELIJK ONDERZOEK TNO
INERIS	INSTITUT NATIONAL DE L ENVIRONNEMENT INDUSTRIEL ET DES RISQUES - INERIS
IOS-PIB	INSTYTUT OCHRONY SRODOWISKA - PANSTWOWY INSTYTUT BADAWCZY
FZJ	FORSCHUNGSZENTRUM JULICH GMBH
AU	AARHUS UNIVERSITET
ENEA	AGENZIA NAZIONALE PER LE NUOVE TECNOLOGIE, L'ENERGIA E LO SVILUPPO ECONOMICO SOSTENIBILE

3 Deposition in global CAMS and associated uncertainties

3.1 Deposition related problematic

Atmospheric removal processes are governed by wet scavenging and dry deposition. Precipitation removes atmospheric species, including critical water-soluble nutrients like ammonium (NH_4^+) and nitrate (NO_3^-), as well as dissolved iron forms (ferrous and ferric organic ligands), all of which can impact vegetation productivity. Gases and particles can settle onto surfaces, including reactive nitrogen gases like ammonia (NH_3) and nitrogen oxides (NO_x), which can also interact with vegetation and soils. Nutrient-containing aerosols, such as Fe and P-containing mineral dust aerosols, are also significantly influenced by sedimentation, which affects their lifetime during long-range transport. However, compared to wet deposition fluxes, dry deposition fluxes are often more variable and frequently affected by nearby activities, such as agricultural or urban emissions.

Desert dust deposition poses a significant challenge to the efficiency of solar panels, particularly in arid and semi-arid regions. As fine dust particles settle on the surface of photovoltaic modules, they scatter and absorb incoming sunlight, drastically reducing the amount of solar radiation that reaches the solar cells. This phenomenon, known as "soiling," can diminish energy output by as much as 20–50% in some extreme cases, depending on dust composition, climate conditions, and the frequency of precipitation and cleaning. Over time, this not only reduces the overall energy yield but also increases operational and maintenance costs, as regular cleaning is required to restore performance. The impact is especially pronounced during dry seasons or dust storm events, making soiling one of the key performance-limiting factors for solar installations in desert environments.

Atmospheric nutrient deposition plays a critical role in both and marine ecosystems (GESAMP; 2022), enhancing productivity in high-nutrient, low-chlorophyll oceanic regions and impacting Earth's carbon cycle. Nitrogen and sulphur deposition in the global ecosystem originates largely from human activities such as consumption of fossil fuels, production and usage of fertilizers, and livestock cultivation, and may increase by a factor of ~2.5 from 2000 to 2100 (Lamarque et al., 2005). Increased nitrogen deposition can cause exceedance of critical loads on ecosystems (Sun et al., 2020). Elevated sulphur and nitrogen deposition are also associated with a host of environmental issues such as acidification and eutrophication of the terrestrial system, while increasing nitrogen deposition could enhance the carbon uptake by land processes (Reary et al., 2008; Holland et al., 1997).

3.2 Deposition in global CAMS

IFS-COMPO, the global atmospheric composition forecasting system used in the global CAMS systems, produces experimental products of wet and dry deposition for a wide range of particulate and gaseous species. Ongoing efforts in CAMS and CAMEO to evaluate these products against observational datasets. Wet deposition in cycle 49R1 is parameterized following Luo et et al (2019), using as input the 3D concentration of the species of interest and liquid and solid precipitation fluxes. Reevaporation is taken into account, following De Bruine et al (2018). As a first order, wet deposition of a given species depend on its burden and on simulated precipitation. Dry deposition of particles in IFS-COMPO is parameterized as a function of particle size, surface type and wind speed following Zhang and He (2014). Dry deposition of gaseous species is adapted from Wesely et al (1989). More details on the IFS-COMPO deposition parameterizations can be found in the cycle 49R1 documentation, available at https://www.ecmwf.int/en/elibrary/81630-ifs-documentation-cy49r1-part-viii-atmospheric-composition .

3.3 Estimating deposition uncertainties through an ensemble approach

A number of factors can lead to errors and uncertainties in deposition products. Uncertainties can arise from:

- Meteorological variables such as wind, temperature and precipitation, which impact directly wet and dry deposition, but also indirectly, as changes in meteorology can also impact emissions (desert dust, sea-salt aerosol) or production (sulfate, nitrate).
- Emissions : in addition to the emissions computed online for desert dust and sea-salt, emissions from many sectors are provided by monthly emission files. Estimating emissions is hard and can be subject to large uncertainties, which directly impact in return simulated deposition. Work package 5 provided some estimates of the uncertainty of temporal profiles of emissions.
- Initial conditions : The initial conditions of each forecast can be more or less erroneous which, depending on the lifetime of the species considered can have a more or less significant impact on the simulated values.
- Model error: many atmospheric composition processes, including wet and dry deposition, are represented in a simplified way in IFS-COMPO. These errors can combine in a non-linear way; processes concerned include dry and wet deposition, the representation of desert dust and sea-salt aerosol emissions, chemical photolysis, chemical reaction rates, etc.
- Desert dust emission scheme inputs: apart from the dust emission scheme, a high degree of uncertainty affects its inputs, i.e. the assumed geographically varying silt, sand and clay fraction of the soil, the dust source function used to correct dust emissions, and the size distribution used at emissions.

In work package 6, a global atmospheric composition ensemble based on IFS-COMPO has been developed and tested, which is described in Section 4. This IFS-COMPO ensemble allows for a quantification of the propagation of uncertainties arising from the different sources of uncertainties listed above on the IFS-COMPO output, including deposition products.

4 Implementation of a global atmospheric composition ensemble forecasting system

ECMWF is producing ensemble weather forecasts since 1992. An ensemble weather forecast is a set of forecasts that present the range of future weather possibilities. Multiple simulations are run, each with a slight variation of its initial conditions and with slightly perturbed weather models (Figure 1). These variations represent the inevitable uncertainty in the initial conditions and approximations in the models. They produce a range of possible weather conditions. Here we would like to extend the existing weather ensemble to atmospheric composition, by using the IFS-COMPO (Integrated Forecasting System with atmospheric composition extensions) instead of IFS in the existing ensemble architecture, and by introducing optional perturbations of initial conditions, emissions and model processes that are specific to atmospheric composition, and aim to represent the impact of uncertainties not related to meteorology.

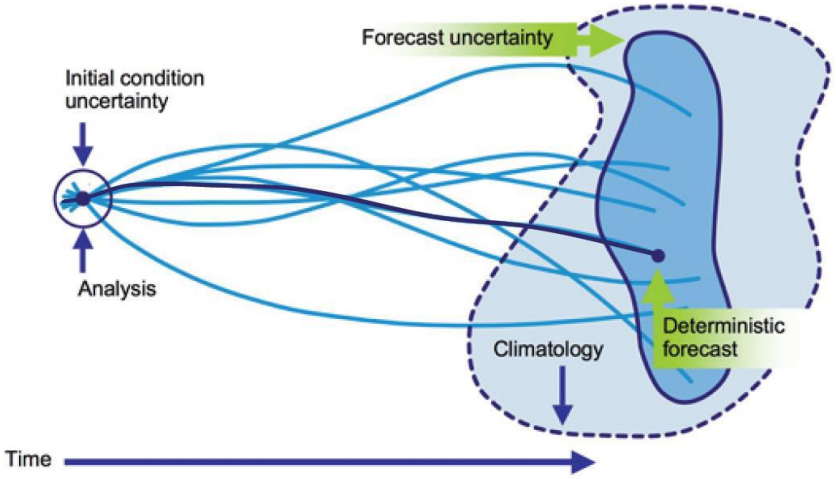

Figure 1: Schematic showing the principles of ensemble forecast. (Julia Slingo and Tim Palmer, 2011, http://doi.org/10.1098/rsta.2011.0161)

4.1 Description of the IFS-COMPO ensemble

The IFS-COMPO ensemble is built on the NWP ensemble in a cycle 48R1 configuration: they include a single control or unperturbed run, and 50 perturbed members. The IFS-COMPO version used in this work is cycle 48R1 but including the aerosol and chemistry developments that have been implemented into cycle 49R1. As such, the results are valid for cycle 49R1, but using cycle 48R1 meteorology and meteorological ensemble perturbation. The ensemble uses an analysis field as initial conditions, so including aerosol and chemistry data assimilation. The perturbations applied to the meteorological fields are those of the IFS meteorological ensemble, described in the cycle 48R1 documentation (https://www.ecmwf.int/en/elibrary/81371-ifs-documentation-cy48r1-part-v-ensemble-prediction-system). They consist of perturbations of the meteorological initial conditions, which are provided from an ensemble of data assimilations (EDA), and perturbations constructed from the leading singular vectors. Model uncertainties are represented in the meteorological ensemble with the Stochastically Perturbed Parameterization Tendencies scheme (SPPT). It simulates the effect on forecast uncertainty of random model errors due to the parametrized physical processes. The SPPT scheme is described in detail in the cycle 48R1 documentation

(https://www.ecmwf.int/sites/default/files/elibrary/2023/81371-ifs-documentation-cy48r1-part-v-ensemble-prediction-system.pdf). It perturbs the meteorological tendencies by terms that are given by a generic random pattern, times the net parameterized physics tendencies, less the diagnosed clear-sky heating rate. The random pattern varies horizontally (but not vertically) and with time; each ensemble member uses a different realisation of the random pattern.

On top of the meteorological perturbations, which are using already existing features of the NWP ensemble, the following set of perturbations have been implemented:

- Perturbations of the initial conditions of all aerosol and selected (carbon monoxide, ozone, sulphur dioxide and nitrogen dioxide) chemistry tracers in the troposphere
- Perturbation of the inputs of the dust emission scheme: dust source function (DSF), sand/silt/clay fraction of the soil used for dust emissions and assumed size distribution at emissions
- Perturbation of the anthropogenic emission inputs of IFS-COMPO
- Perturbation of atmospheric composition specific model parameterizations:
    - Computation of dry deposition velocity
    - Rates of chemical reactions
    - Photolysis rates
    - Wet deposition and re-evaporation rates
    - Production rate of sulphate and nitrate aerosols
    - Production rate of secondary organic aerosols
    - Emissions of desert dust and sea-salt aerosols

Ensemble simulations can be carried out using all or a selection of the perturbations presented above. Also, we developed the possibility to run ensemble simulations without perturbations of meteorological initial conditions and parameterizations, so as to allow to assess the impact of the uncertainties of atmospheric composition specific inputs and processes. It should be noted that **perturbations of different input/parameterizations are assumed to be uncorrelated, and perturbations are supposed to be constant for all forecasts time**, which is a strong (and probably wrong) assumption. In addition to this, for the relevant perturbations (initial conditions, model components), the perturbations are similar over the vertical. The perturbations themselves consist of 2D fields that represent correlated gaussian noise, computed using a given correlation length and standard deviation. They are computed on-the fly using a python script that is called in the IFS-COMPO scripts, and are applied to each relevant model input (emissions, initial conditions, etc.). For the model parameterizations, two such stochastic perturbations are computed, loaded into IFS-COMPO, and used in the IFS-COMPO Fortran code to scale the output of the parameterizations listed above. Figure 2 shows an example of such a perturbation.

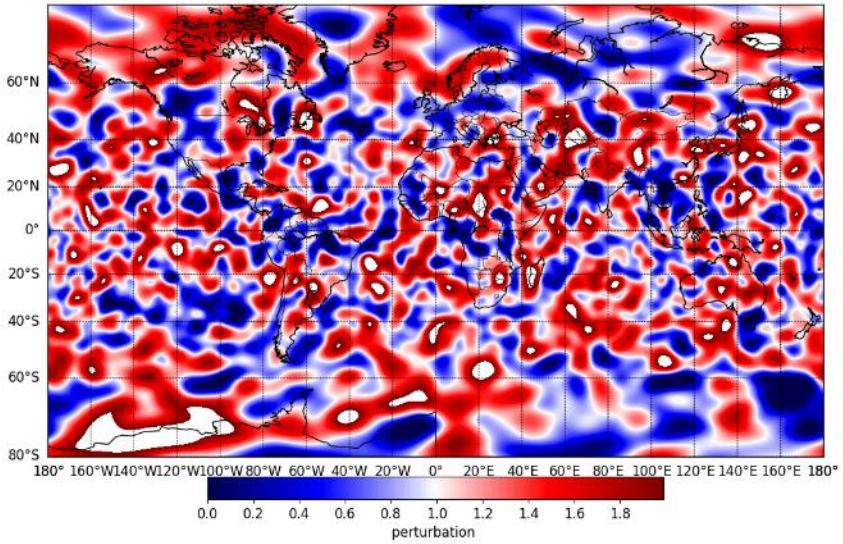

Figure 2: Example of a perturbation scaling factor generated with a correlation length of 500km and a standard deviation of 0.5.

Table 1 lists the specifics of the perturbations applied to the atmospheric composition initial conditions, the inputs of the dust emission scheme and the model parameterizations. These values have been obtained by evaluating how dispersive the ensemble is, depending on the specifics of the input perturbations. For the initial conditions, it was found that higher standard deviations could make ensemble simulations over dispersive for long lived species, such as carbon monoxide and ozone, and much lower values have been used for later simulations.

Table 1: Standard deviation and correlation length of the random perturbations applied to different inputs and parameterizations of the IFS-COMPO ensemble

Perturbed field	Standard deviation of perturbation factor (unitless)	Correlation length of perturbation factor (km)
Aerosol initial conditions	0.25	500
CO initial conditions	0.04	500
O_3 initial conditions	0.07	500
NO_2 initial conditions	0.125	500
SO_2 initial conditions	0.19	500
Model parameterizations	0.5	500
Inputs of the dust emission scheme	0.5	500

Simulations have been carried out with correlation lengths varying between 250 and 2000km, in order to check the sensitivity of the ensemble spread on this particular parameter. The impact of the perturbation correlation length on the ensemble spread, averaged monthly and over the globe, was found to be very small. Those runs led to the selection of correlation lengths presented in Table 1. A special treatment has been implemented for the perturbation of emission input, detailed in the next subsection.

4.1.1 Perturbation of emission input

For emissions, sectoral perturbations are used, i.e., the perturbations are the same for the emissions of all the species of a given emission sector. This is a strong assumption which is most likely erroneous; however, as we don't have more information about the uncertainties of the emissions of specific species for the same sector, there was no choice but to use this hypothesis.

Work package 5 delivered at the end of May 2024 estimates of the temporal uncertainties of anthropogenic emissions. For more details on how these estimates were computed, please refer to deliverable D5.1. These consist of global values representing the standard deviation for each hour for the diurnal cycle uncertainties, and gridded monthly standard deviation to represent the uncertainty of the seasonal cycle. These two sets of standard deviations are provided for each emission sector. An example of the monthly standard deviation is shown in Figure 3 for the energy sector.

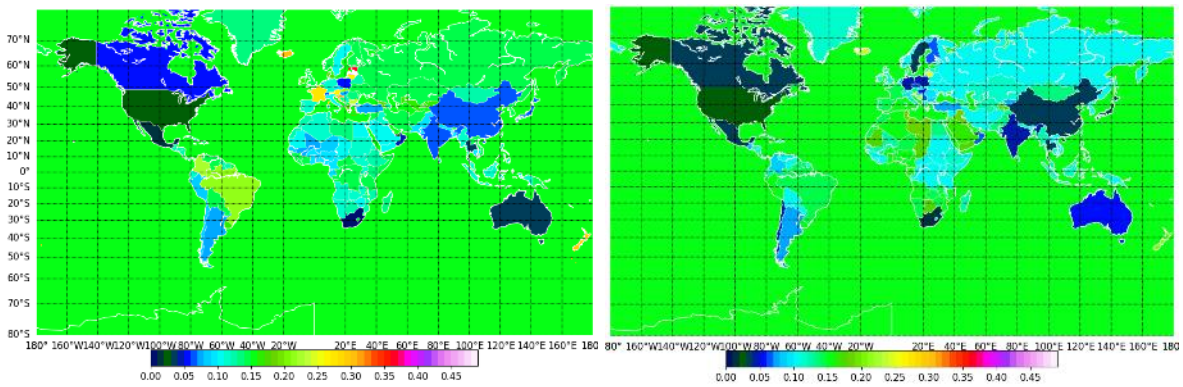

Figure 3: Standard deviation in emissions from the energy sector, January (left) and July (right).

Following the advice of the WP5 leader, the maximum value of the uncertainty standard deviation of the diurnal cycle was used. The values are summarized in Table 2.

Table 2: Standard deviation of the uncertainty of anthropogenic emissions, per sector.

Sector	Standard deviation of correction factor
Ind/Industry	0.15
Res/Residential	0.487
Agl/Agriculture	0.451
Awb/Agriculture waste burning	1.233
Ene/Energy	0.063
Tro/Transport	0.397
Fef/Fugitives	0.25
Slv/Solvents	0.375
Tnr/Non road transport	0.469
Swd/Solid waste	0.25
Shp/Ship	0.25

These values are used, with a correlation length of 500km, to generate perturbation files. On top of this, the gridded monthly values are used to modulate the perturbations, by scaling the perturbation over each grid cell by the gridded monthly value divided by the spatial average of the gridded monthly value. An example is shown in Figure 4, for the energy sector in January. The higher perturbations over Iceland and Estonia/Latvia correspond to areas where the gridded values that represent the seasonal uncertainty spread for this month are the highest, as shown in Figure 3.

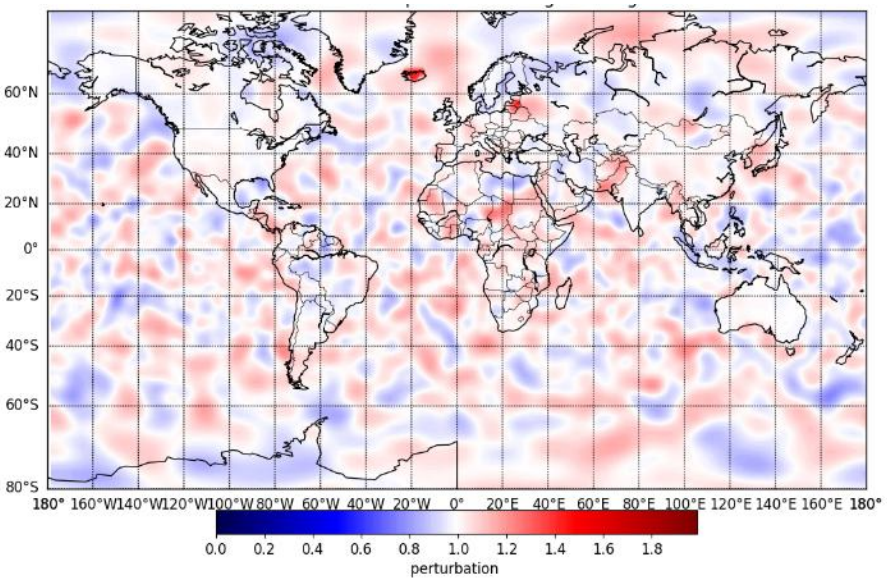

Figure 4: Example of a perturbation scaling factor for emissions from the energy sector in January.

The perturbations of emissions computed following this methodology only represent the temporal uncertainties as provided by WP5. They don't include other aspects of emissions uncertainties, relating to activity data used to compute the emissions, conversion factors etc. is not taken into account, which means that it is very possible that the emissions uncertainties, as represented by the estimated perturbations are underestimated.

4.2 Experiments

A number of experiments have been carried out in order to evaluate and adjust the perturbations applied to initial conditions, emissions and model parameterizations, which are not shown here. The ensemble simulations use initial conditions (before perturbation) from analysis simulations from cycle 48R1 for the year 2021. They use a cycle 48R1 branch, which includes modelling updates for cycle 49R1. As such, the uncertainties shown are representative of the uncertainties of the official cycle 49R1 products, but for the year 2021.

The experiment specifics are the following:

- T_L255L137 resolution (80km grid cell)
- 120h maximum forecast time, output every 12 hours
- Simulated year 2021
- Use of CAMS_GLOB_BIOv3.1 and CAMS_GLOB_ANT v5.3 emissions

Because of the high computing costs of the IFS-COMPO ensemble experiments, most of them didn't complete the year 2021. We chose to show results for experiments that perturb i) only meteorological fields, ii) only anthropogenic emissions, iii) only model parameterizations, and iv) all uncertainties combined. For desert dust, the experiment that perturbs the inputs of the dust emission scheme is also shown instead of the one that perturbs anthropogenic emissions.

The choice of experiments was made so as to isolate and describe clearly the impact of each possible perturbation family (meteorology, emissions, model, desert dust emission scheme inputs), and to compare the impact of each of these perturbations to the impact of their full combination (experiment ALL). The experiments are listed in Table 3.

Table 3: IFS-COMPO ensemble experiments shown in this report

Experiment	Characteristics
MET	Perturbations of meteorological initial conditions and processes
EMI	Perturbations of anthropogenic emissions input only, using WP5 input
MODEL	Perturbation of atmospheric composition model parameterizations only: • Computation of dry deposition velocity • Chemical reaction rates • Photolysis rates • Wet deposition and re-evaporation rates • Production rate of sulphate and nitrate aerosols • Production rate of secondary organic aerosols • Emissions of desert dust and sea-salt aerosols
ALL	All perturbation applied: • Meteorological initial conditions and processes • Atmospheric composition initial conditions • Atmospheric composition model parameterizations • Inputs of the dust emission scheme • Anthropogenic emission input using WP5 input
DUST	Perturbation of the inputs of the dust emission scheme : • dust source function • fraction of soil composed of silt and clay • assumed size distribution at emissions
ALL_NOMODEL	All perturbations applied except model parameterizations
INI	Perturbation of atmospheric composition initial conditions only

Experiments will be shown in the following sections based on their relevance, not all experiments will be included. In particular, the estimated deposition uncertainties will be shown for MET, EMI, MODEL and ALL, and for DUST instead of EMI for desert dust.

5 Evaluation of the ensemble forecasts

The raw ensemble forecasts look like the stamp plot shown in Figure 5, which shows how a situation with high PM10 from a desert dust plume over South of France and Northern Italy is simulated by an IFS-COMPO ensemble simulation. These plots include a lot of information; however, it can be hard to compare simulations from one ensemble against another, or even two different simulations of the same ensemble. To do this, metrics that incorporate information from all ensemble members are needed, such as the ensemble standard deviation or spread and ensemble median. Examples of these two quantities are shown in Figure 6 for surface ozone from two IFS-COMPO ensembles: MET and ALL, for a single day that saw high ozone concentrations over most of Europe. The ensemble median is very similar for the two experiments, with an area of values above 100 µg/m^3 that covers most of Western Europe. The spread of MET is relatively small, between 2 and 5 µg/m^3 in general, which shows that the meteorological perturbations have relatively little impact on simulated ozone on that day. The spread is significantly higher for ALL, with values generally between 10 and 15 µg/m^3 over most of Europe, which indates that ozone perturbations are sensitive to other perturbations than meteorology.

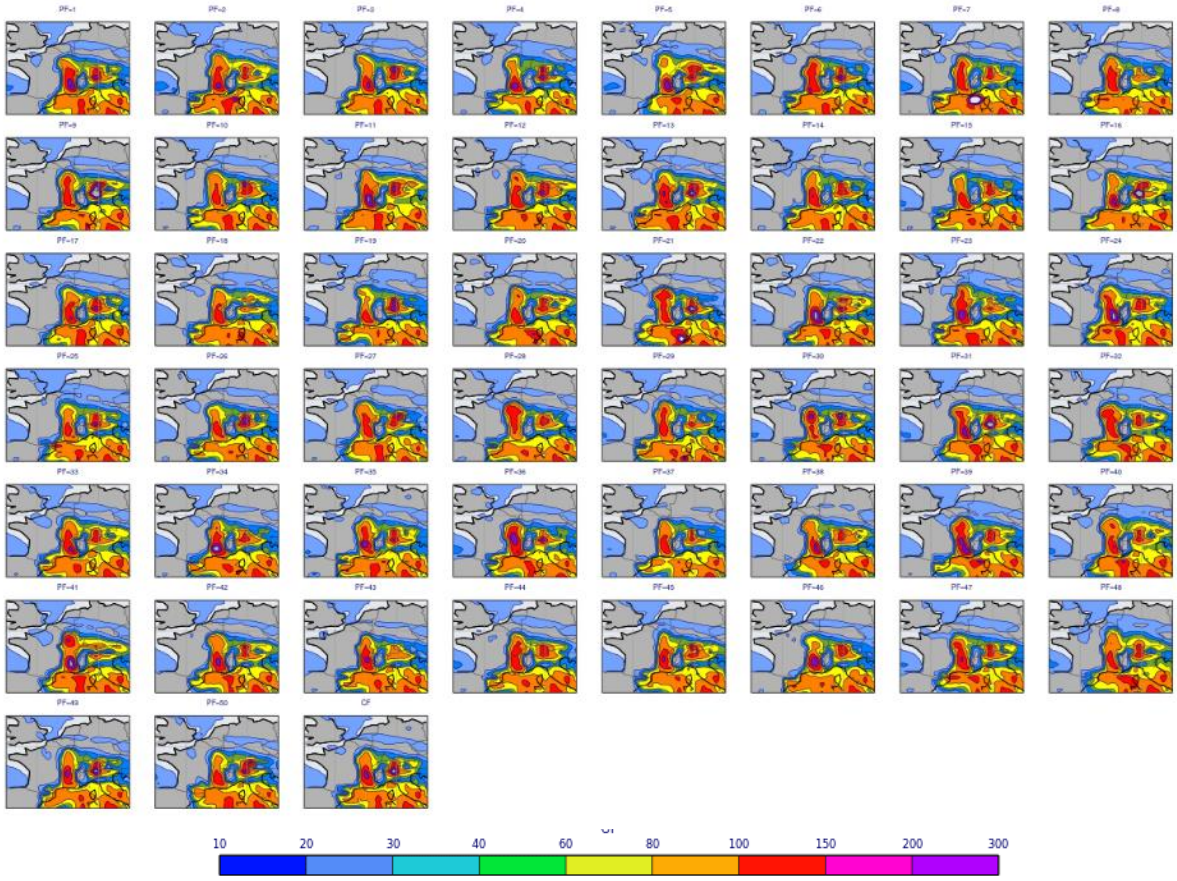

Figure 5: Simulated PM10 in microg/m^3 at 24h forecast time over Western Europe, simulation starting on 6/2/2021, IFS-COMPO ensemble perturbing meteorology only.

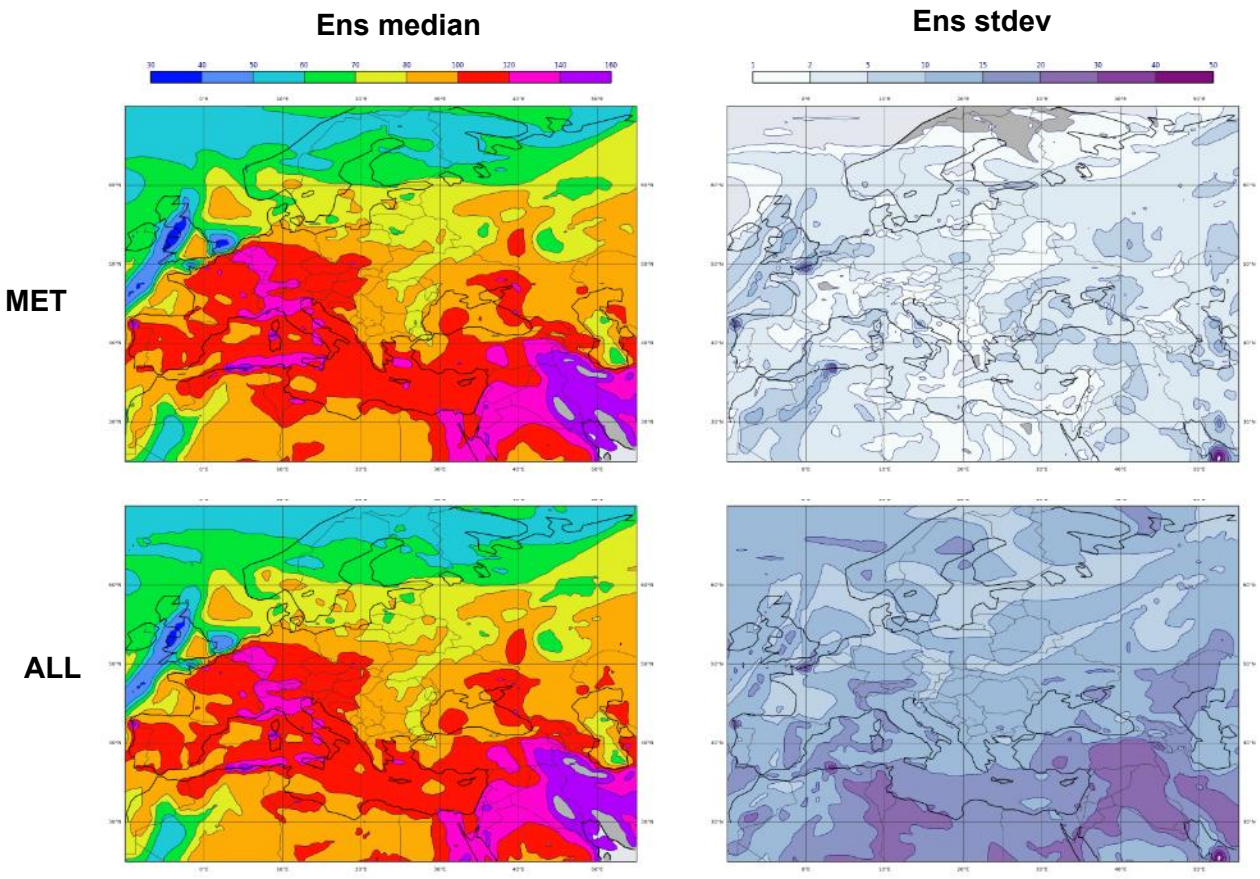

Figure 6: IFS-COMPO ensembles MET (top) and ALL (bottom), surface ozone at 36h forecast, run starting on 15/6/2021. Ensemble median (left) and standard deviation/spread (right).

Comparing the spread of two ensemble simulations is a good way to assess how sensitive the model is to perturbations of each kind of input. However, this doesn't give any information if the spread is "too low" or "too high". For this, skill scores that involve observational datasets are required. We implemented two different metrics

- A comparison of ensemble spread and the root mean square error (RMSE) of the ensemble mean,
- Rank histograms (Talagrand diagrams),
- Comparison of simulated and observed probability density functions.

It is common practice to assess the skill of an ensemble by comparing the ensemble mean RMSE and the ensemble standard deviation (ensemble spread). We chose this approach over other possible ensemblist verification metrics such as CRPS and its Hersbach decomposition, etc. The former measures how accurate the ensemble mean is, i.e. how near the mean of the ensemble forecasts is to analysis fields or observations; the latter verifies whether the ensemble forecasts simulated a wide enough range of possible atmospheric states to reflect the error characteristics of the ensemble mean. Ideally, one would want the ensemble mean RMSE to be as small as possible and the spread to be equal to the ensemble mean RMSE on average over many cases.

For the verification of ensemble forecasts the Rank histograms (also called Talagrand diagrams) are widely used. This type of diagram shows how often observations match different parts of an ensemble forecast distribution. To this end, the ensemble forecast distribution is divided into bins of equal size, matching the ensemble size (or number of members), for example going from low predicted to high predicted AOD at 550nm. The observations are then

put in the appropriate bins forming a histogram. In a reliable ensemble forecast, the frequency of observations in each bin will be identical since each part of the ensemble forecast distribution is equally likely. Figure 7 show three examples of simulated and observed probability distributions along with rank histograms. When the ensemble is well calibrated the rank histogram is roughly flat. High values at the extremes diagnose an ensemble with too little spread, also called under dispersive. A biased ensemble will show a slope. Finally, an over-dispersive ensemble (not shown) will show high values in the middle ranks, and null or lower values at the extremes.

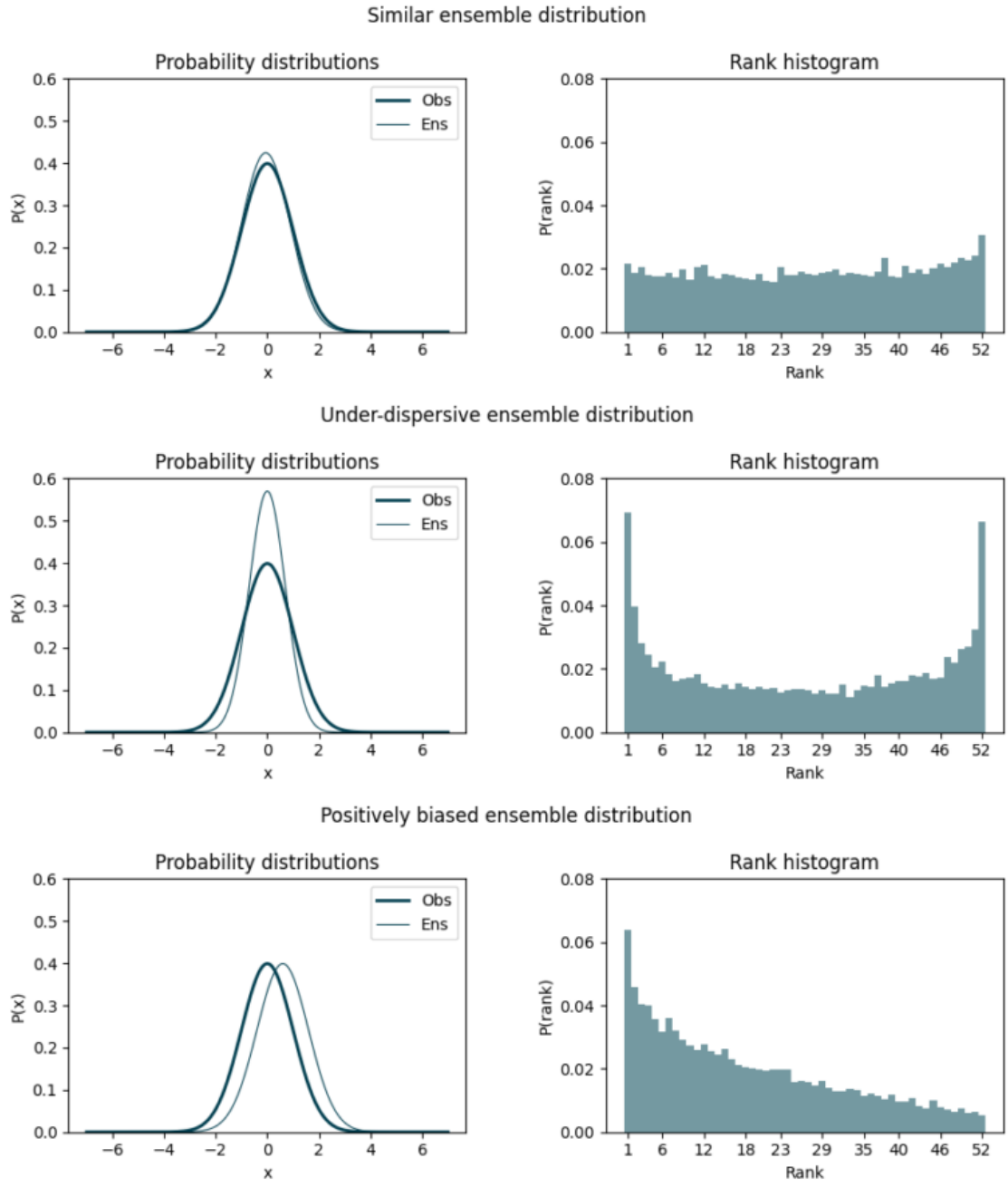

Figure 7: Three examples of probability distribution and rank histograms, showing well balanced (top row), under-dispersive (middle row) and biased situations (bottom row).

This ensemblist scores can be computed using either an observational dataset, or against their own analysis. Each approach has its benefits and drawbacks. Using the ensemble

analysis for verification is more adequate for assimilated quantities (such as AOD) than for non assimilated species, as the analysis is then deemed more reliable. Using this method for PM2.5 or surface ozone for example is not advised (at least as long as they are not assimilated), as the link between the analysis and observations is indirect in the global CAMS system. Using its own analysis for verification is also very convenient because the model space and the observation space are the same; there are no resolution or representativeness issues. Verification against observational datasets offer a better reference than against own analysis; however, the data can be sparse and there can be representativeness issues between observation and model. In this section, we present rank histograms computed against both observational datasets and own analysis.

5.1 Rank histograms (Talagrand diagrams)

5.1.1 AOD at 550nm

Figure 9 shows the observed and simulated frequency distribution, a rank histogram and a time series of observed versus simulated Aerosol Optical Depth (AOD) at 500nm for the ALL experiment in February 2021, for a 120h forecast time. The evaluation is done against all AERONET level 2 data available in February 2021. The AERONET network is shown in Figure 8.

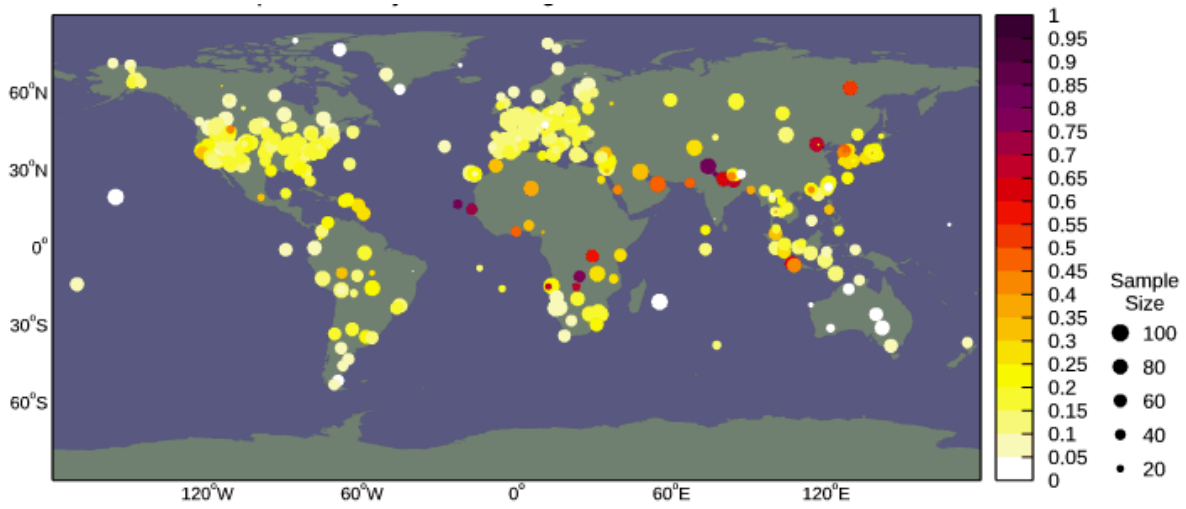

Figure 8: AERONET level 2 AOD at 500nm in the summer of 2020, values and sample size.

The rank histogram shows that for AOD and this experiment, the IFS-COMPO ensemble is clearly under dispersive: a significant amount of observations falls outside of the 50 members and are above the maximum values out of the 50 members (high value for entry 50 in the X axis). This is also shown by the lower ensemble standard deviation (0.15) as compared to the observation standard deviation (0.19). The ensemble suffers also from a negative bias, which is also apparent in the time series: both the control and ensemble mean are most of the time below the observational average because of a persistent low bias of the control run over the considered period. As such, the low bias shown here is rather a consequence of inherent model bias, also present in the control run. However, the ALL experiment lacks the ability to represent a significant fraction of the observed space for AOD at 550nm.

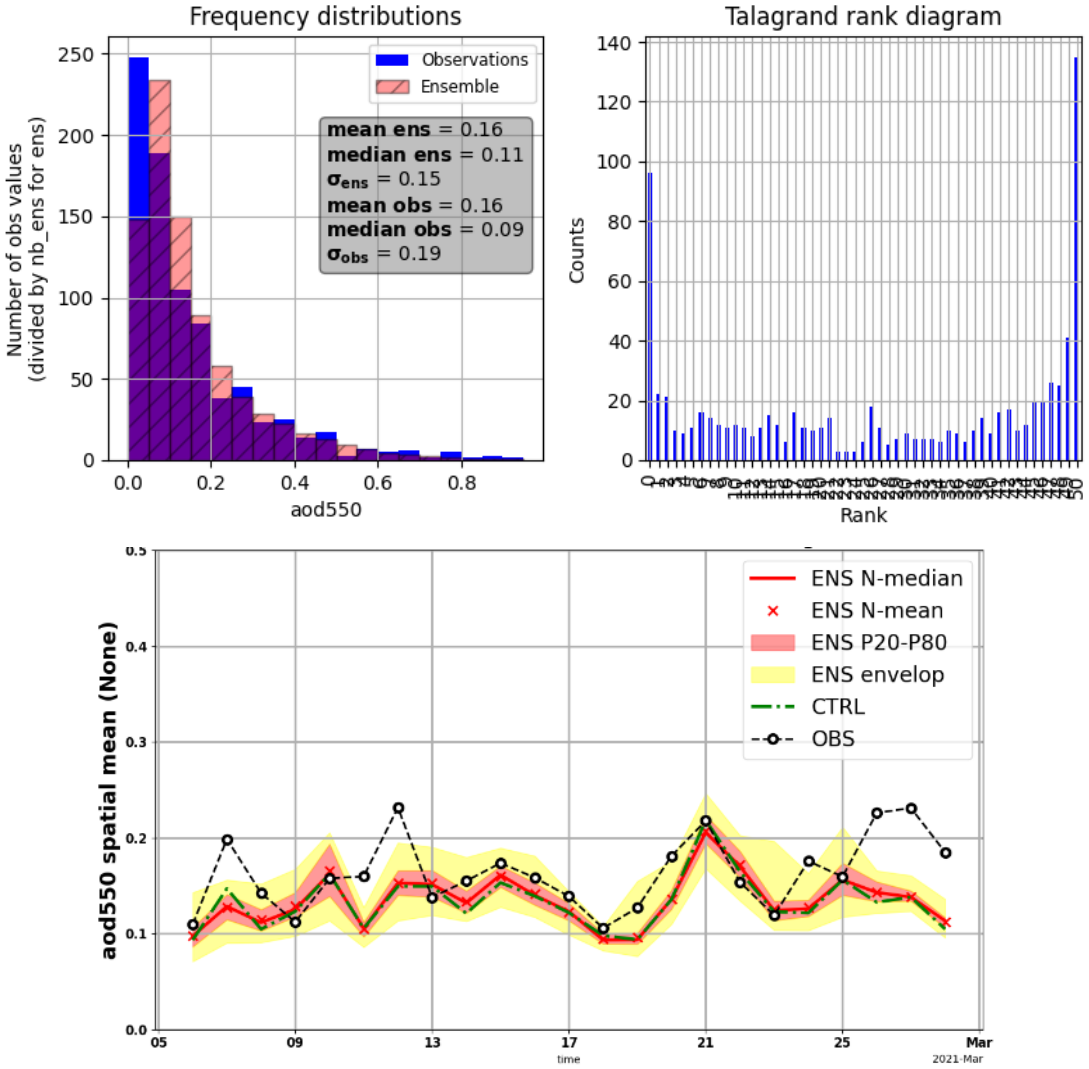

Figure 9: ALL experiment, February 2021, 120h forecast time, evaluation of AOD at 550nm versus all AERONET level 2 observational data. Top left, frequency distribution; top right, rank histogram. Bottom, time series of daily observed mean AOD at 550nm averaged over all AERONET stations together with the ensemble mean and median and values simulated by the control run. The ensemble 20% and 80% centiles as well as the envelope are shown.

Figure 10 shows a similar global evaluation of a series of IFS-COMPO ensemble simulations by a rank diagram, but against their own analysis instead of against observations, for AOD at 550nm simulated at 120h forecast time. The diagnostic is similar to that reached against AERONET: all of the ensembles are more or less under dispersive for AOD. However, at the global scale, there is no sign of a positive or negative bias (this is not the case for the regional evaluation, not shown). The EMI and INI experiments are significantly more under dispersive than the MET one, showing that for AOD, the perturbations applied to the atmospheric composition initial conditions as well as anthropogenic emissions yield relatively little ensemble spread. The ALL_NOMODEL experiment is slightly less under dispersive than MET, but by a small margin: this shows that meteorological perturbations have the largest impact on ensemble spread for AOD, as the spread of the ensemble perturbing meteorology and of the ensemble perturbing all source of uncertainties apart from model error are quite similar (perturbations of the atmospheric composition model parameterizations were not evaluated in this context).

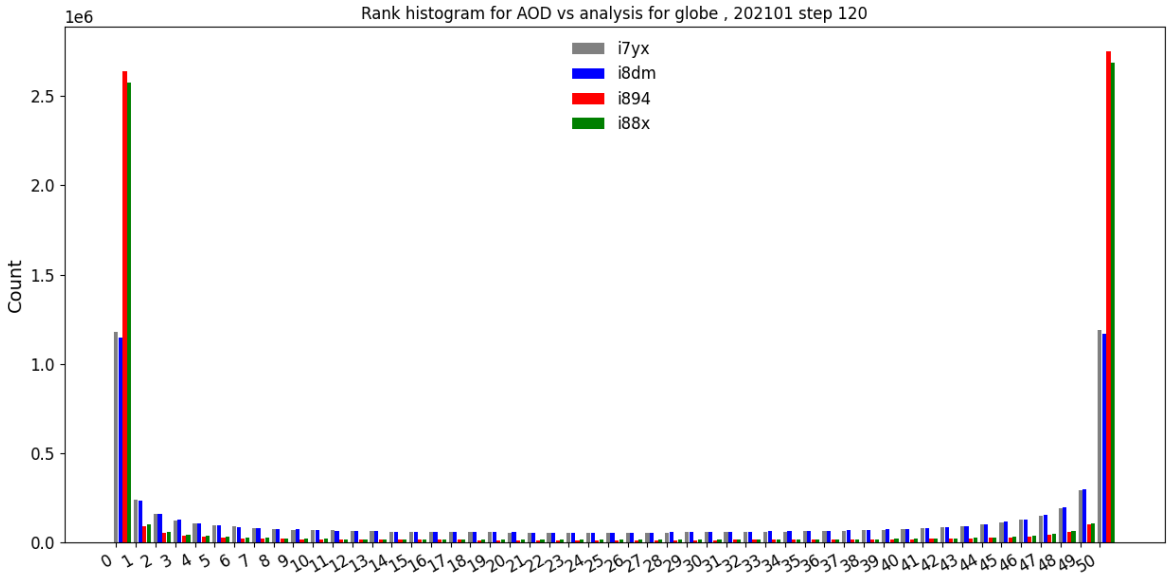

Figure 10: January 2021, 120h forecast time, evaluation of AOD at 550nm versus own analysis. Rank histogram of MET (grey), ALL_NOMODEL (blue), EMI (red), and INI (green).

5.1.2 PM2.5

Rank histograms have been built also for PM2.5 against European airbase/EEA stations, for simulated PM2.5 at 120h forecast time in February 2021 by the MODEL and ALL experiments (Figure 11). The two experiments are under-dispersive and negatively biased, although the under-dispersion is less pronounced for the ALL experiment. This negative bias is very apparent in the time series, which shows that up to 20/21 February 2021, the control run and ensemble mean PM2.5 are significantly lower than the observational average. The MODEL experiment struggles to reach observed values even for the maximum ensemble values, while the ALL experiment sometimes manages to reach the observed value. The period 20-25 February 2021 was marked by a combined pollution and dust intrusion event over most of Western and Central Europe, which is reflected in the higher observed average PM2.5. The simulated values are less impacted by a low bias during this period.

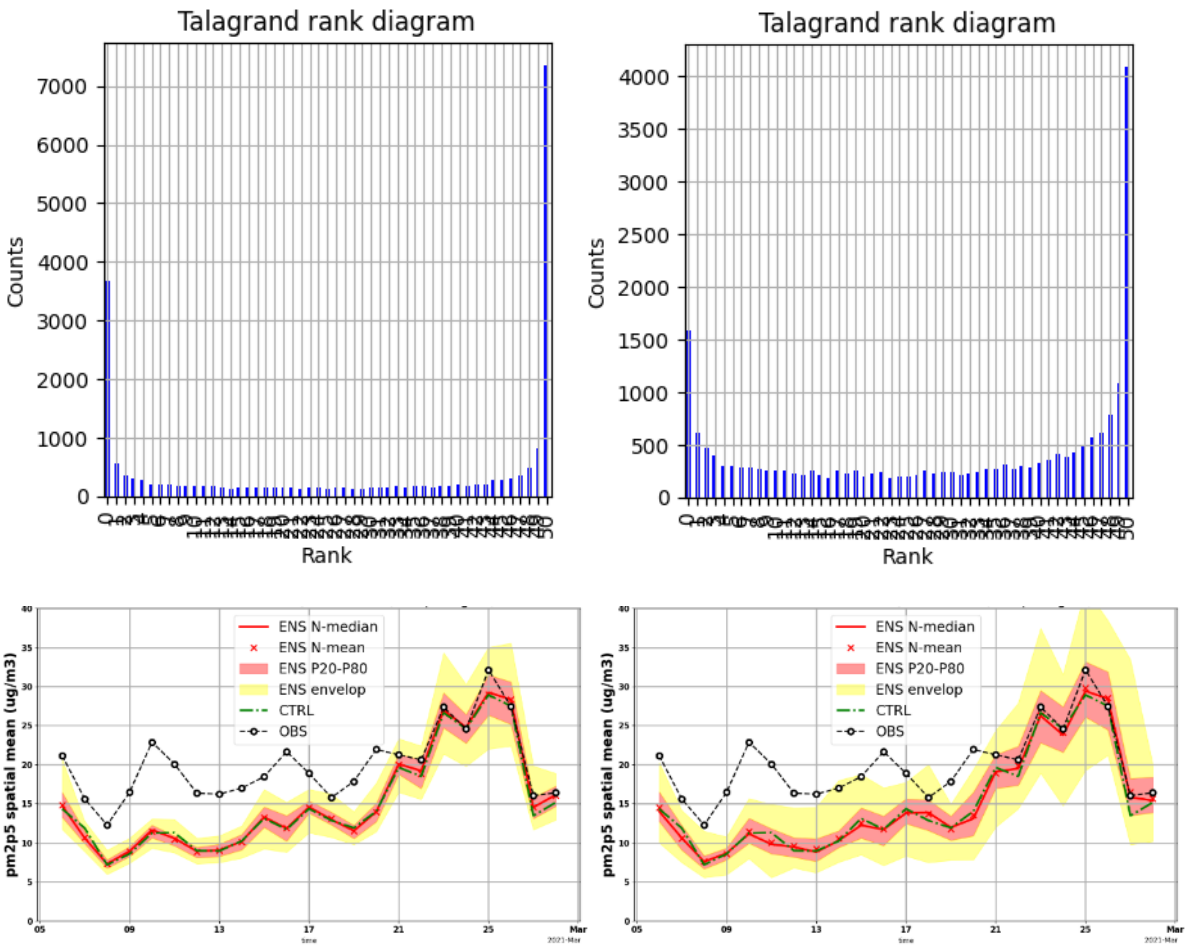

Figure 11: Top, rank histograms of MODEL experiment (left) and ALL experiment (right), February 2021, 120h forecast time, evaluation of PM2.5 versus all available airbase/EEA data over Europe. Bottom, time series of daily observed mean PM2.5 in February 2021 over European stations together with the ensemble mean and median and values simulated by the control run. The ensemble 20% and 80% centiles as well as the envelope are shown.

6 Uncertainties of selected CAMS deposition products

In this section, we present monthly average standard deviation and relative standard deviation (normalized by the ensemble mean value) of IFS-COMPO ensembles MET, DUST, MODEL and ALL for a selection of species. We focused on the following species:

- Desert dust, because its deposition is of importance to many users, and also to study how perturbations of the online dust emissions are propagated to deposition uncertainties,
- Sulfate, because of its impact on soil and precipitation acidity,
- Organic matter, a good tracer of anthropogenic pollution as well of fire events,
- Nitric acid, a gaseous precursor of nitrate aerosols.

The uncertainty of the sum of dry deposition and sedimentation is shown, as well as wet deposition. For wet deposition of particles, we show only the contribution from large scale precipitation, as it is by far the dominant contribution. For nitric acid, total wet deposition is shown. The standard deviation, or ensemble spread, is taken as a measure of the uncertainty of the simulated products. Other measures are possible, such as the difference between the 25 and 75% percentiles. The spread is shown for two months, February and May 2021, and also at 24h forecast time and 120h forecast time (for May 2021, only 120h forecast time is shown), in order to assess how forecast time impacts the uncertainty of deposition products. We chose to show monthly values, as the daily variability is very high, particularly for wet deposition, which depends on simulated precipitation fields. The values shown for February and May 2021 differ for absolute spread, but are usually rather similar for relative spread. Other months also show values in the same range for relative spread: the results shown in this section can qualitatively be extended to other months as far as relative spread is concerned.

6.1 Desert dust

In this subsection, the simulated uncertainty of dust deposition (total, dry and wet deposition) are discussed.

6.1.1 Total deposition

Figures 12, 13 and 14 show the ensemble spread and relative spread of desert dust total deposition from the MET, DUST, MODEL and ALL experiments, for February 2021 and for 24 and 120h forecast time, and for May 2021 only 120h forecast time except for MODEL and ALL for which data is incomplete for that month. The absolute total dust uncertainty depends primarily on the simulated dust burned and surface concentration : values reach around 0.1 kg/m²/year over the major source areas (Sahara, middle East), and decrease sharply over outflow regions. For total dust deposition at 24h forecast, the uncertainty caused by meteorological factors and model perturbations is much higher than the uncertainty arising from the inputs of the dust emission scheme. This is also because those uncertainties (of the inputs of the dust emission scheme) propagated only over 24h of forecast, so are limited to regions close to source areas. At 120h forecast times, the uncertainties from the inputs of the dust emission scheme have propagated much farther, as illustrated by the Atlantic for example. The relative spread is highly variable, often higher over continents than over oceans, except for an area of high values along the Equator in the Atlantic Ocean. Values are comprised between 20 and 50% in general, higher over some dust source regions (South Sahara, Taklimakan). The uncertainties arising from meteorology and from model perturbations are quite close in range in general. For DUST, the uncertainties as measured

by the spread is in general between 20 and 30%, with values reaching 50% over specific source areas such as Australia and Taklimakan.

The uncertainty of total dust deposition is unsurprisingly higher for 120h forecasts, with values between 35 (over oceans) to more than 70% for MET and MODEL, while DUST perturbations are generally between 20 and 30% over continents (closer to 50% over some source areas). Some regions with very high relative spread correspond to areas with relatively small absolute spread, indicating that the small value of the ensemble mean contributes to the high value of the relative uncertainty. Also, meteorological perturbations could result in the transport of dust over areas with a low dust burden, which mechanically provokes a very high relative spread. Also, it is clear that the propagation of uncertainties through the IFS-COMPO ensemble is a very non-linear phenomenon: the spread of ALL is smaller than the sum of the spread of MET, MODEL and DUST. Actually, the relative spread of ALL is even lower than that of MET over some regions such as the Eastern Atlantic, which is surprising and can only be explained by meteorology and model perturbations attenuating each other.

In May 2021, the absolute uncertainty is much higher than in February, mostly because simulated dust deposition is higher over many regions. The relative spread is higher over many regions including most of Sahara for MET, but the relative uncertainty of DUST is quite similar between February and May 2021.

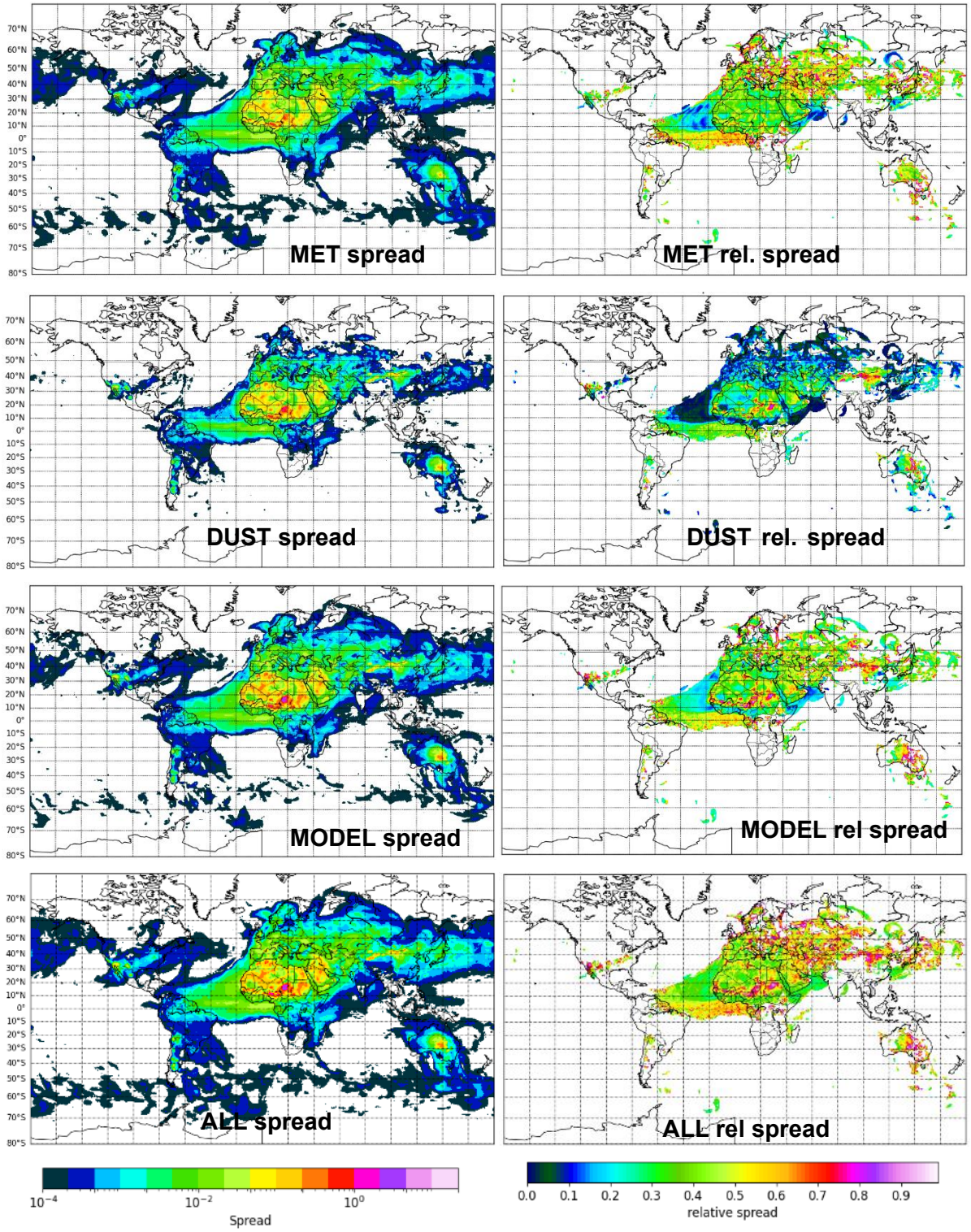

Figure 12: Spread (left) in kg/m²/yr and relative spread (right) of the MET, DUST, MODEL and ALL experiments for simulated dust total deposition in February 2021, at 24h forecast time.

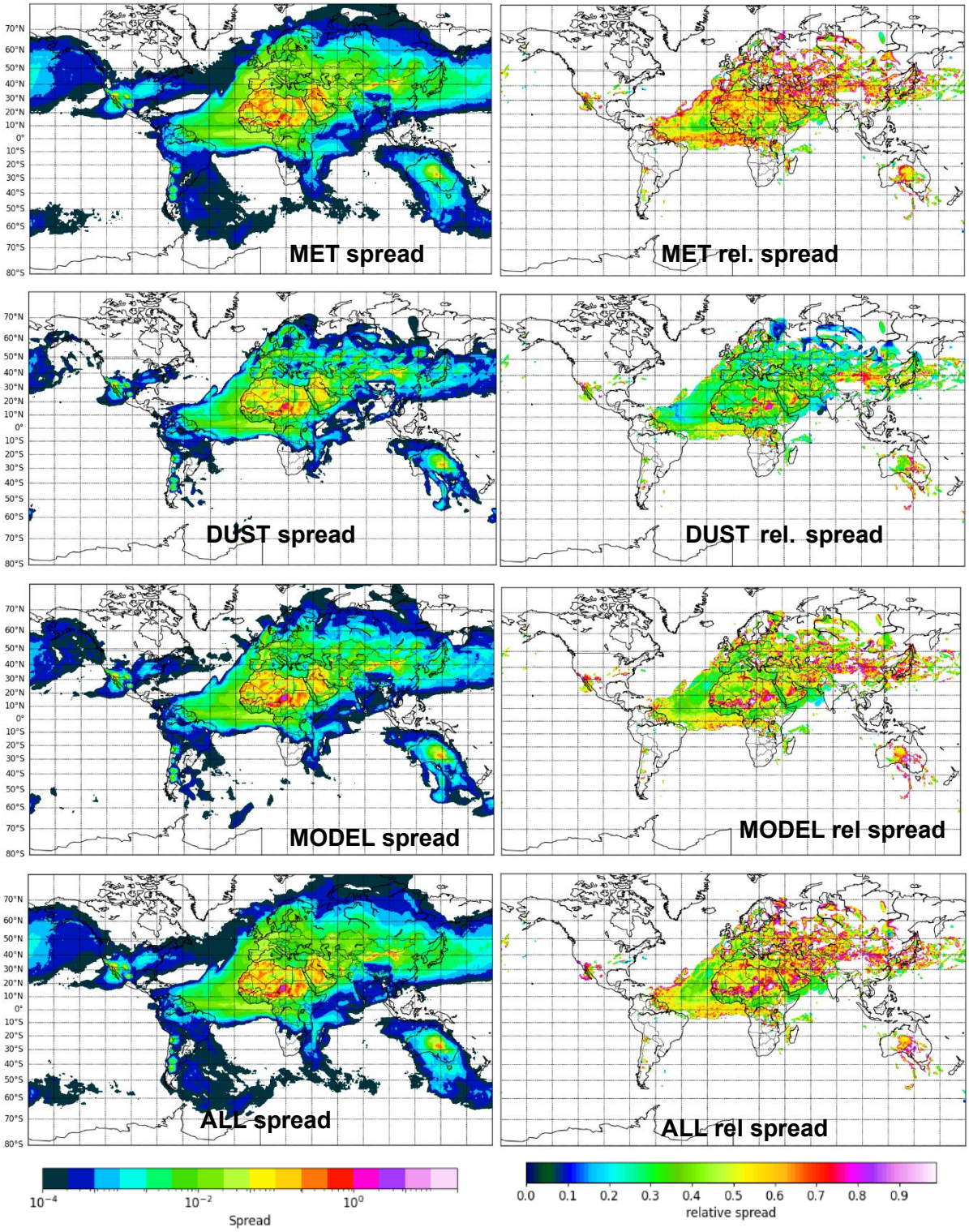

Figure 13: Spread (left) in kg/m²/yr and relative spread (right) of the MET, DUST, MODEL and ALL experiments for simulated total dust deposition in February 2021, at 120h forecast time.

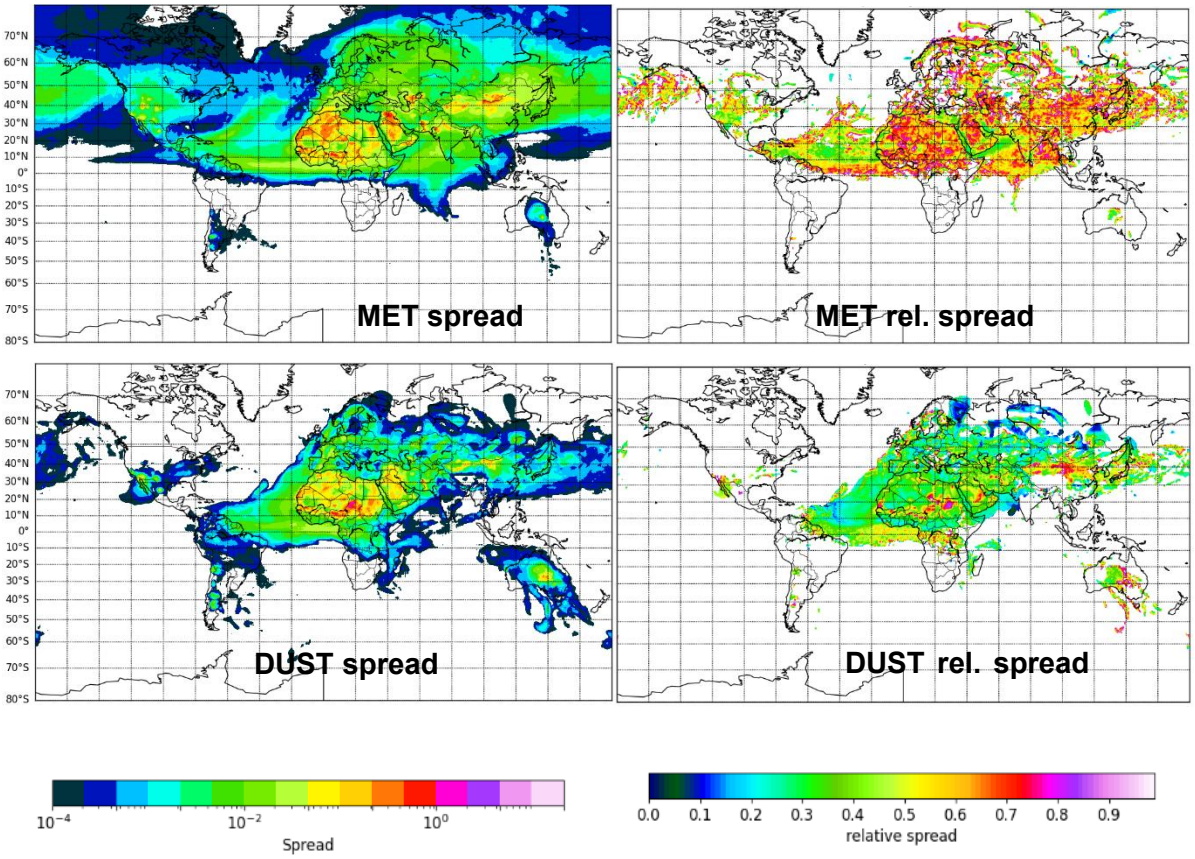

Figure 14: Spread (left) in kg/m²/yr and relative spread (right) of the MET and MODEL experiments for simulated total dust deposition in May 2021, at 120h forecast time.

6.1.2 Dry deposition and sedimentation

In order to better understand the uncertainty of total dust deposition, we will now focus on the sum of desert dust dry deposition and sedimentation in this section, and on wet deposition in next section. For the sum of dust dry deposition and sedimentation (Figures 15, 16 and 17) the EMI experiment is not shown, as its impact is very small. The uncertainty of dust dry deposition and sedimentation is much higher over continents than over oceans for all experiments. This is partly caused by the fact that the dust surface concentration (for dry deposition) and burden (for sedimentation) is usually higher over continents than over oceans. But the relative spread also shows lower values over oceans, which is likely caused by lower uncertainties for dry deposition over smooth surfaces (water) as opposed to higher uncertainties and spread over rough surfaces. The lower values for relative spread over the Atlantic with MET could be also because those areas could be relatively less impacted than regions closer to the main dust emitting areas by the uncertainty arising from dust emissions. Over the main dust emitting regions, the values of absolute and relative spread are similar to those noted for total deposition, showing that over these regions, which see very little precipitation, the bulk of the dust deposition uncertainty comes from dry deposition and sedimentation. At 120h forecast time, the area concerned by higher uncertainties is quite similar between all experiments. The relative spread is close between MET and MODEL, a bit higher for MODEL over the Atlantic at 24h forecast time. The relative spread of ALL at 120h show very similar patterns to MODEL but values only slightly larger. The relative spread is close between February and May 2021.

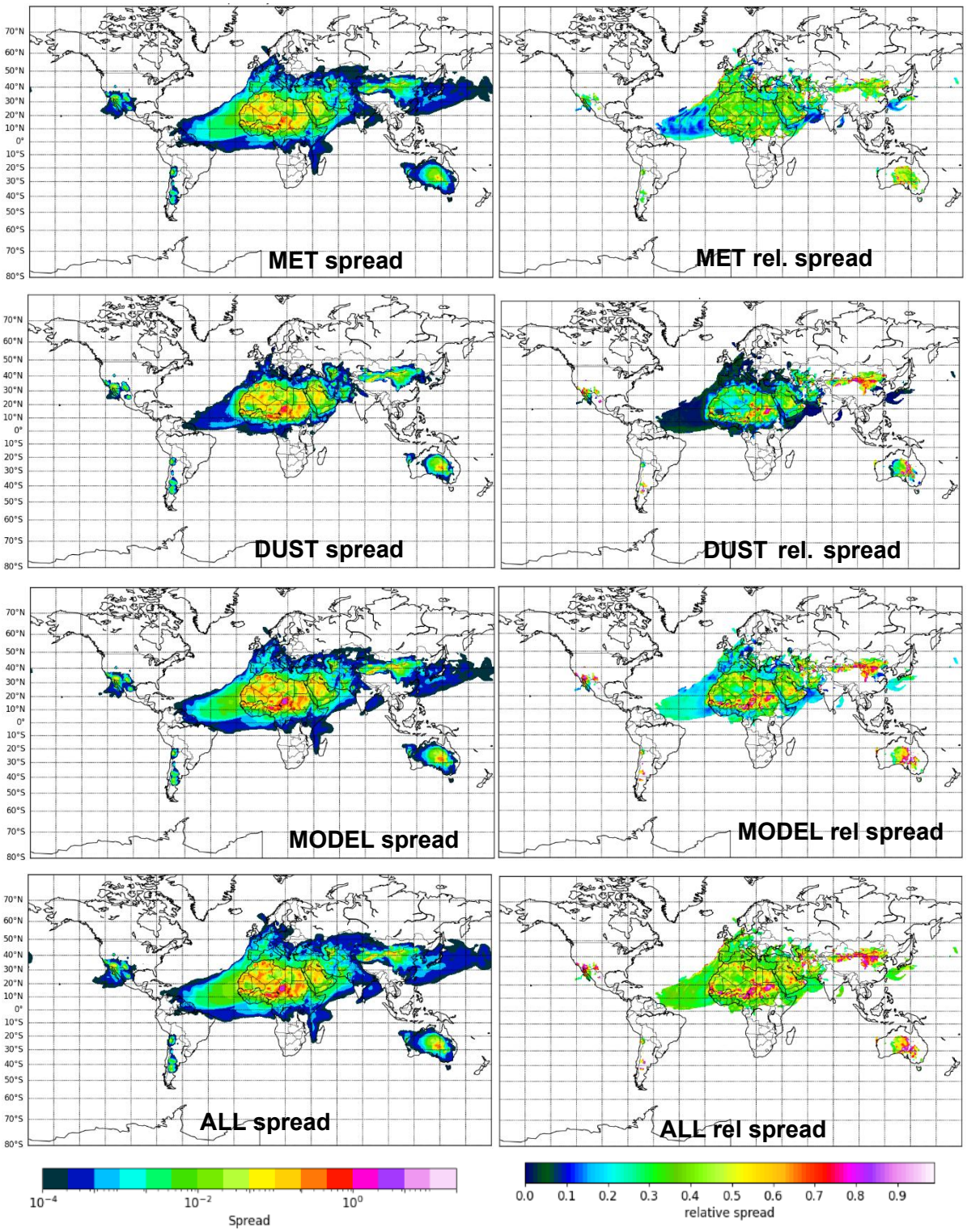

Figure 15: Spread (left) in kg/m²/yr and relative spread (right) of the MET, DUST, MODEL and ALL experiments for simulated dust dry deposition and sedimentation in February 2021, at 24h forecast time.

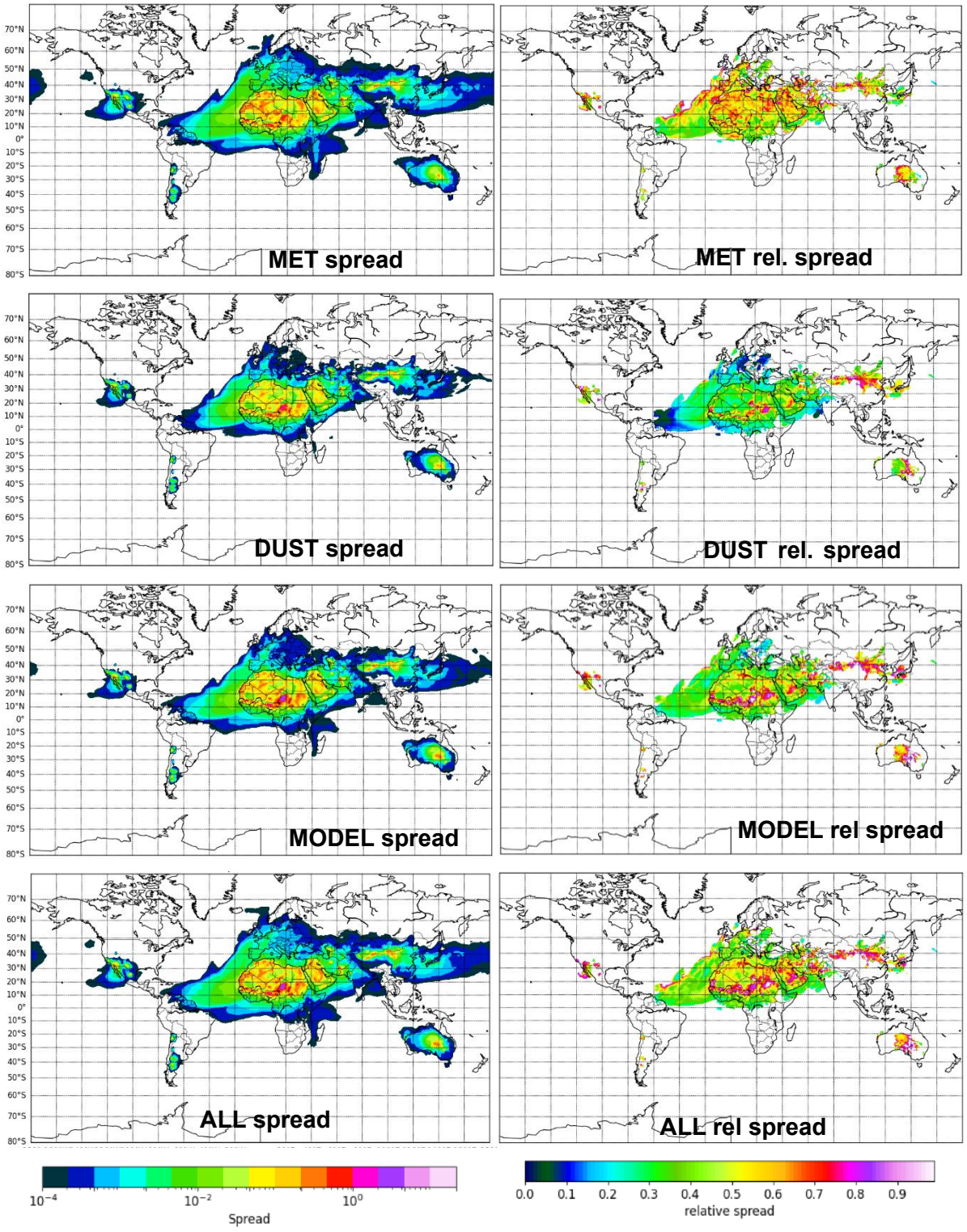

Figure 16: Spread (left) in kg/m²/yr and relative spread (right) of the MET, DUST, MODEL and ALL experiments for simulated dust dry deposition and sedimentation in February 2021, at 120h forecast time.

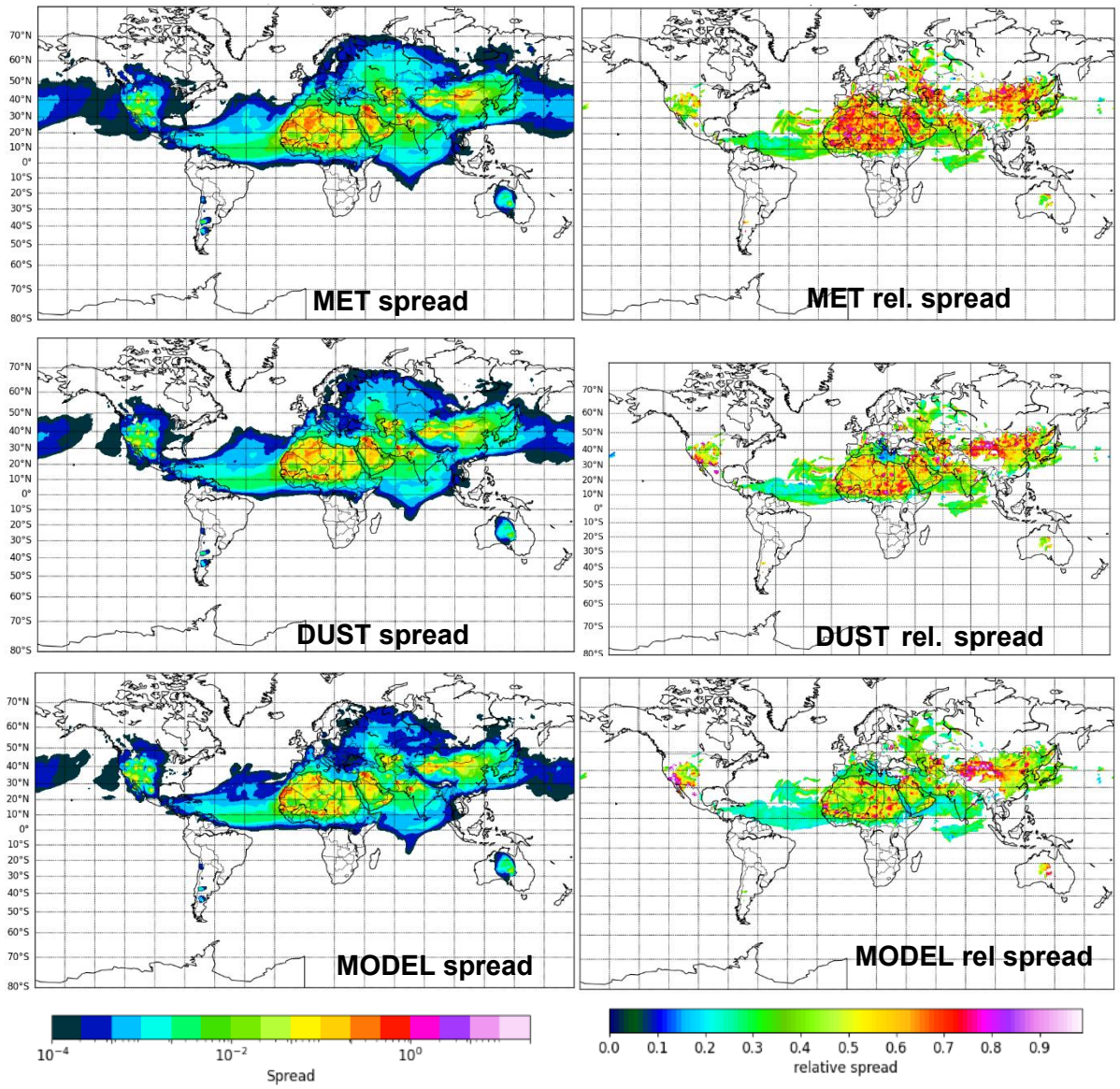

Figure 17: Spread (left) in kg/m²/yr and relative spread (right) of the MET, DUST and MODEL experiments for simulated dust dry deposition and sedimentation in May 2021, at 120h forecast time.

6.1.3 Wet deposition

The patterns of the absolute and relative spread of dust wet deposition (Figures 18, 19 and 20) are very different from those of dry deposition. At 24h and 120h forecast time, the areas with high absolute and relative uncertainty correspond to outflow areas, where dust is transported and subjected to precipitation. In February, the highest absolute uncertainty, comprised between 0.01 and 0.02 kg/m²/year, corresponds to Western Europe, the Middle East, and the Atlantic around the equator. Western Europe in particular was impacted by two large dust events on 6-7 and 20-22 February 2022, with associated wet deposition events. The values are much lower than that of dry deposition absolute uncertainty, because they are concentrated far away from dust sources, where the burden and surface concentrations are much lower than over source regions. The relative spread, on the other hand, shows very high values, between 40 and 60% in general for MET, with a lot of noise. The high values could be partly artificial in the sense that the normalisation to compute the relative spread is done using the control (i.e. unperturbed) run. If precipitation patterns are changed in the ensemble members, as is very likely in particular for the MET experiment, then it is possible to have extremely high relative spread because of a very low normalisation denominator, if precipitations/wet deposition are absent from the control run. Unlike dry deposition, the absolute and relative uncertainty of desert dust wet deposition doesn't increase much with forecast time: the values at 120h forecast time are quite comparable to those at 24h forecast times. The patterns change in May 2021 as compared to February 2021 because dust source and outflow regions change also, but the relative spread is comparable to the February 2021 values.

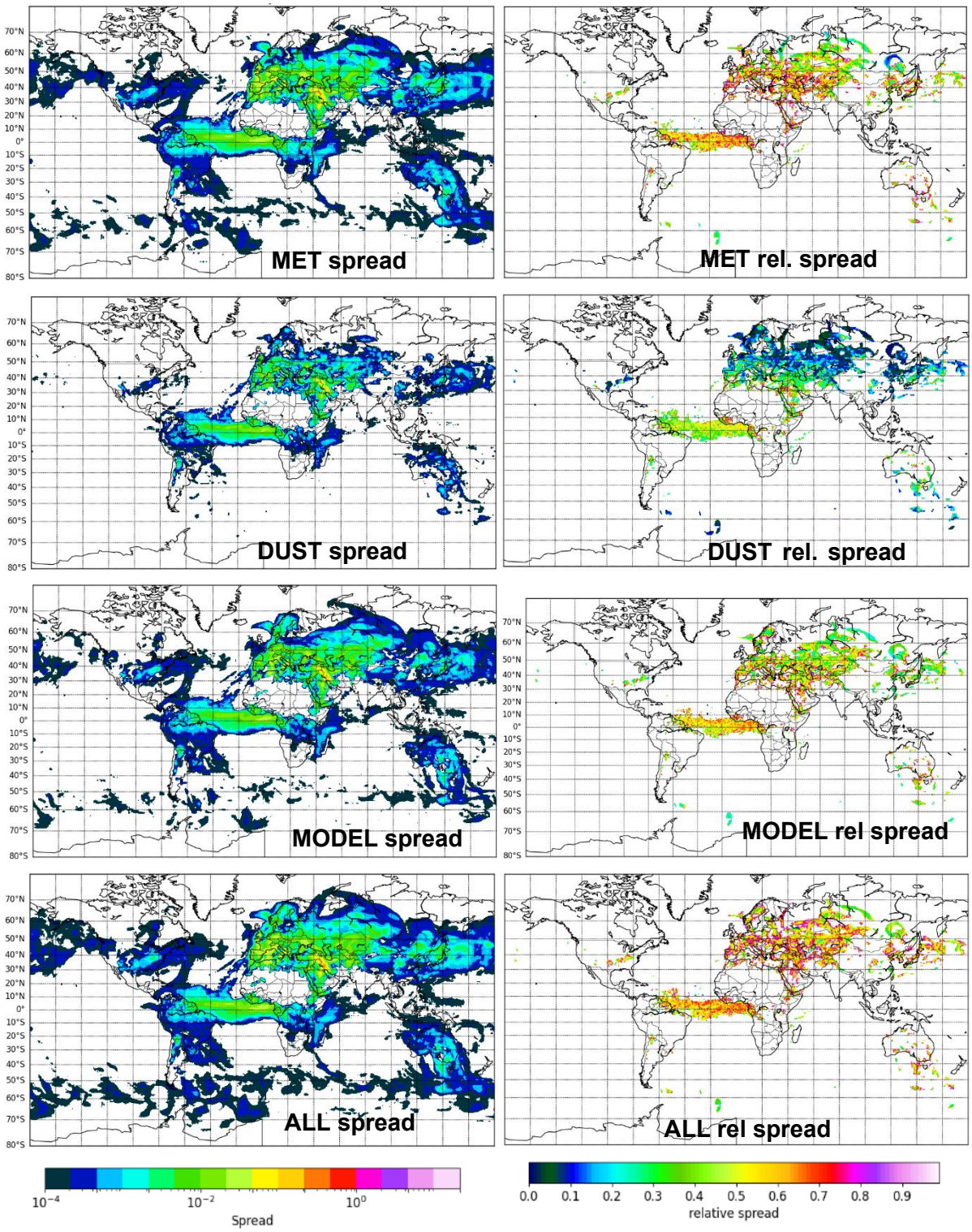

Figure 18: Spread (left) in kg/m²/yr and relative spread (right) of the MET, DUST, MODEL and ALL experiments for simulated dust large scale wet deposition in February 2021, at 24h forecast time.

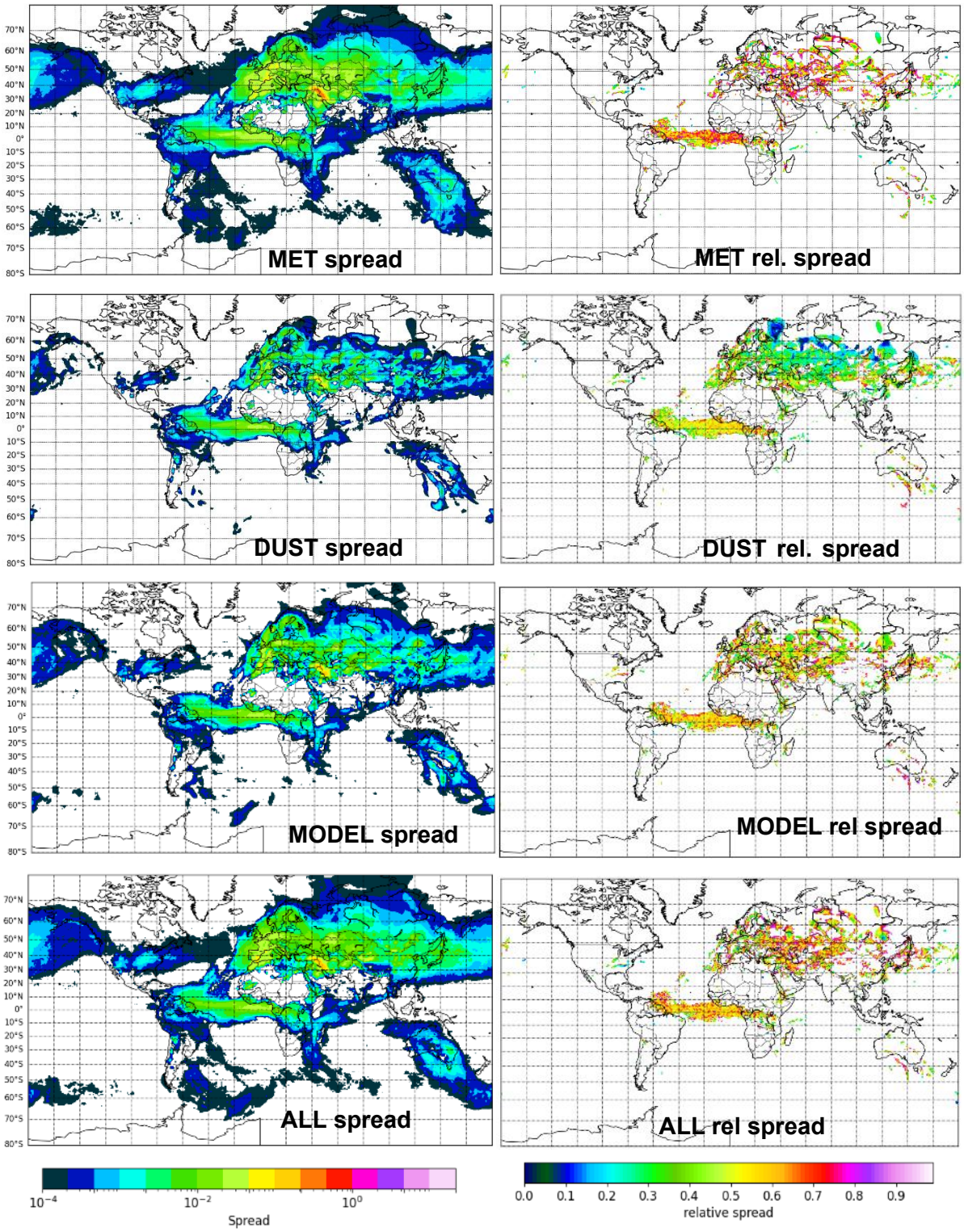

Figure 19: Spread (left) in kg/m²/yr and relative spread (right) of the MET, DUST, MODEL and ALL experiments for simulated dust large scale wet deposition in February 2021, at 120h forecast time.

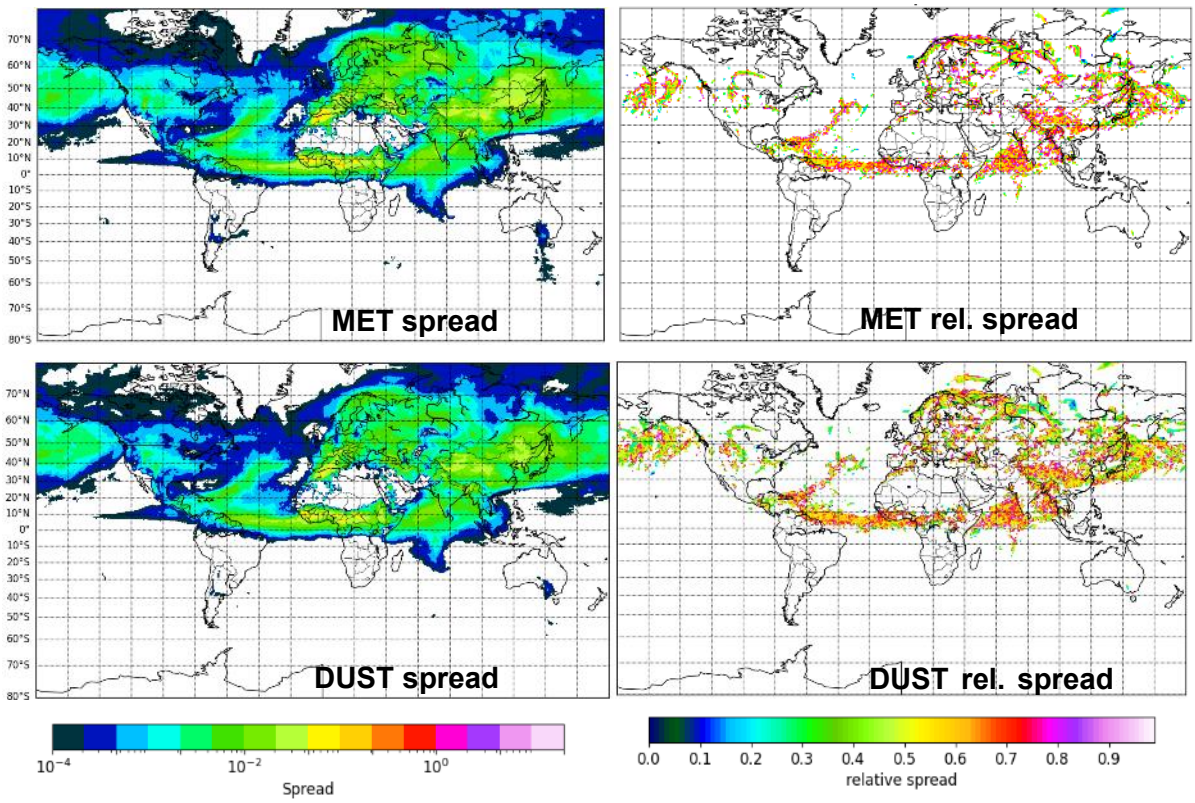

Figure 20: Spread (left) in kg/m²/yr and relative spread (right) of the MET and DUST experiments for simulated dust large scale wet deposition in May 2021, at 120h forecast time.

6.2 Sulfate

6.2.1 Dry deposition

Figures 21,22 and 23 show the ensemble spread and relative spread of sulfate dry deposition fluxes as estimated by the MET, EMI, MODEL and ALL experiments, for Febuary 2021 and for 24 and 120h forecast time, and for May 2021 only 120h forecast time. Sulfate dry deposition occurs over oceans, both from the transport and deposition of sulfate that is produced out of continental anthropogenic emissions, but also in more remote locations (Southern oceans, Pacific, etc.) from the deposition of sulfate produced out of oceanic DMS. This explains the non-negligible uncertainty of sulfate dry deposition over all oceans. The MODEL and ALL experiments show much higher absolute and relative spread than the MET and EMI experiments. The relative spread is often higher over continental regions, with values over 30-40% over Equatorial Africa and Amazon for MET, 10-20% for EMI, and 50-60% for MODEL and ALL. Over oceans, the values of the relative spread are quite homogeneous for all experiments except MEL: at 24 forecast time, they range between 5 and 20% for MET, 0-5% for EMI, 30-40% for MODEL and 40-50% for ALL. At 120h forecast time, the spread and uncertainty increase significantly for MET, EMI and ALL (particularly over extra tropical oceans), less so for MODEL.

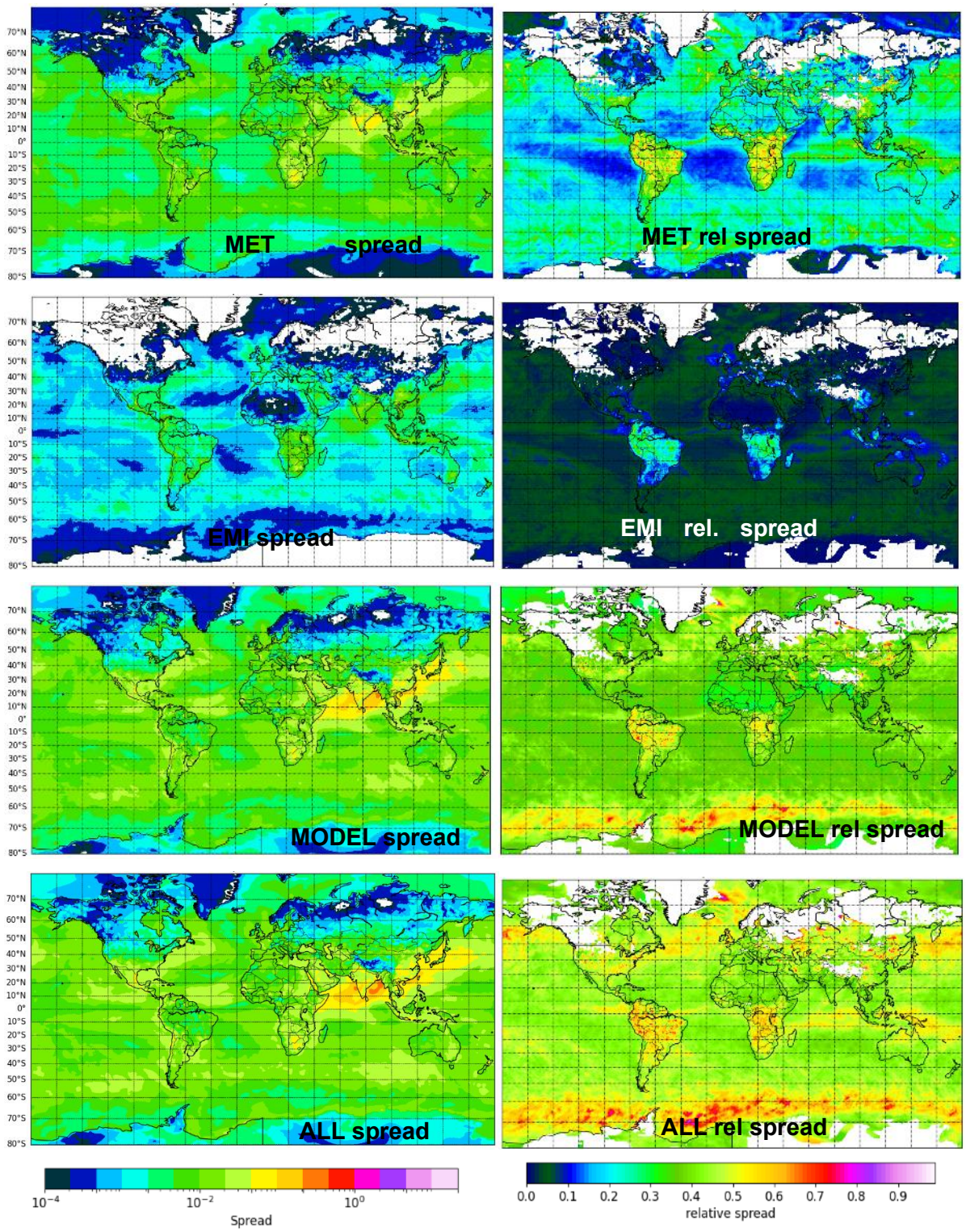

Figure 21: Spread (left) in g/m²/yr and relative spread (right) of the MET, EMI, MODEL and ALL experiments for simulated sulfate dry deposition in February 2021, at 24h forecast time.

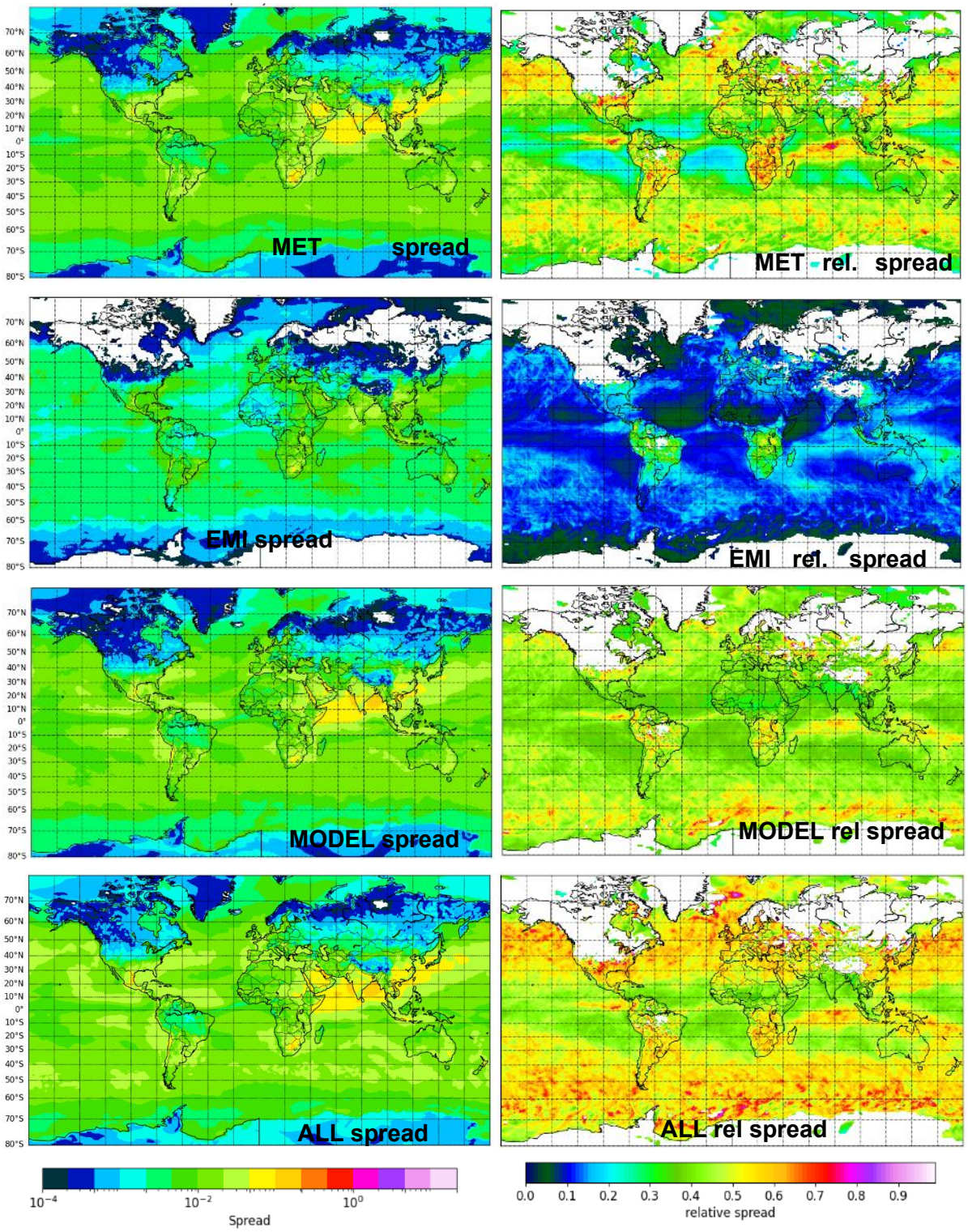

Figure 22: Spread (left) in g/m²/yr and relative spread (right) of the MET, EMI, MODEL and ALL experiments for simulated sulfate dry deposition in February 2021, at 120h forecast time.

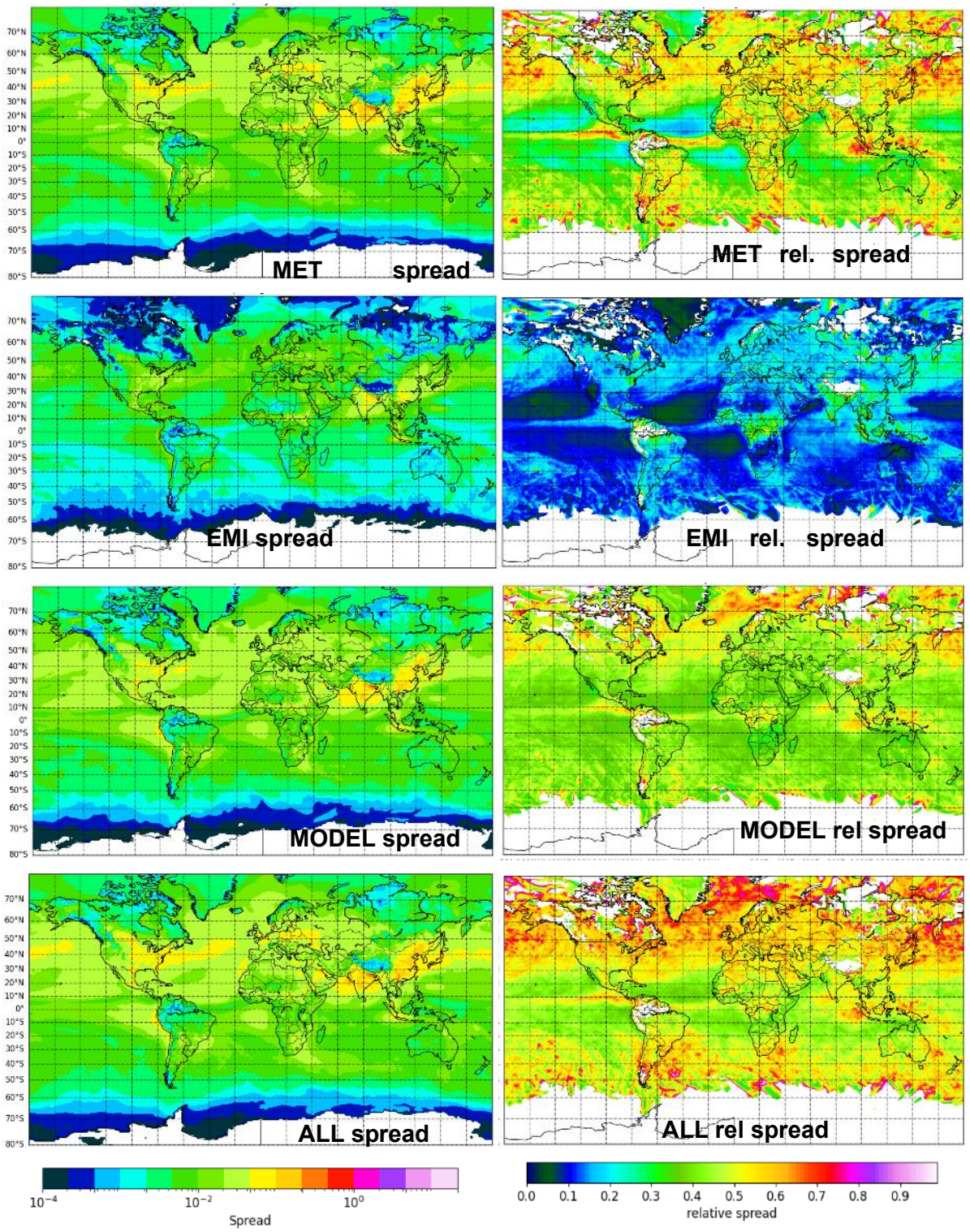

Figure 23: Spread (left) in g/m²/yr and relative spread (right) of the MET, EMI, MODEL and ALL experiments for simulated sulfate dry deposition in May 2021, at 120h forecast time.

6.2.2 Wet deposition

The absolute and relative uncertainty of sulfate wet deposition in February and May 2021 is shown in Figure 24, 25 and 26. Unfortunately, the data to compute the relative spread of MET was not available. The absolute spread is much higher for all experiments than that of dry deposition, which is explained by the fact that for sulfate, wet deposition if, on a global average, a much more efficient sink than dry deposition. For all experiments, the patterns show a combination of regions with high anthropogenic emissions (East Asia, Europe, East US) and with high precipitation (the ITCZ, Southern Oceans). At 24h forecast time, the values are quite similar between MET, MODEL and ALL, reaching 0.5 to 1 g/m²/year over the most impacted regions. The relative spread is very noisy over areas with relatively low precipitations, probably because of the reasons noted above (very low values of wet deposition from the control run which serves as the denominator to compute the relative spread). Over regions with frequent precipitations, such as the extra tropical oceans, the noise is less significant, and the mean values are comprised between 20 and 30% for EMI, and 30-50% for MODEL. Both the noisy aspect and the mean values increase significantly with forecast time. The patterns of the absolute uncertainty change quite a lot in May 2021 as compared to February, with much higher values over Europe and Siberia for example, but the relative uncertainty show values in the same range as in February 2021.

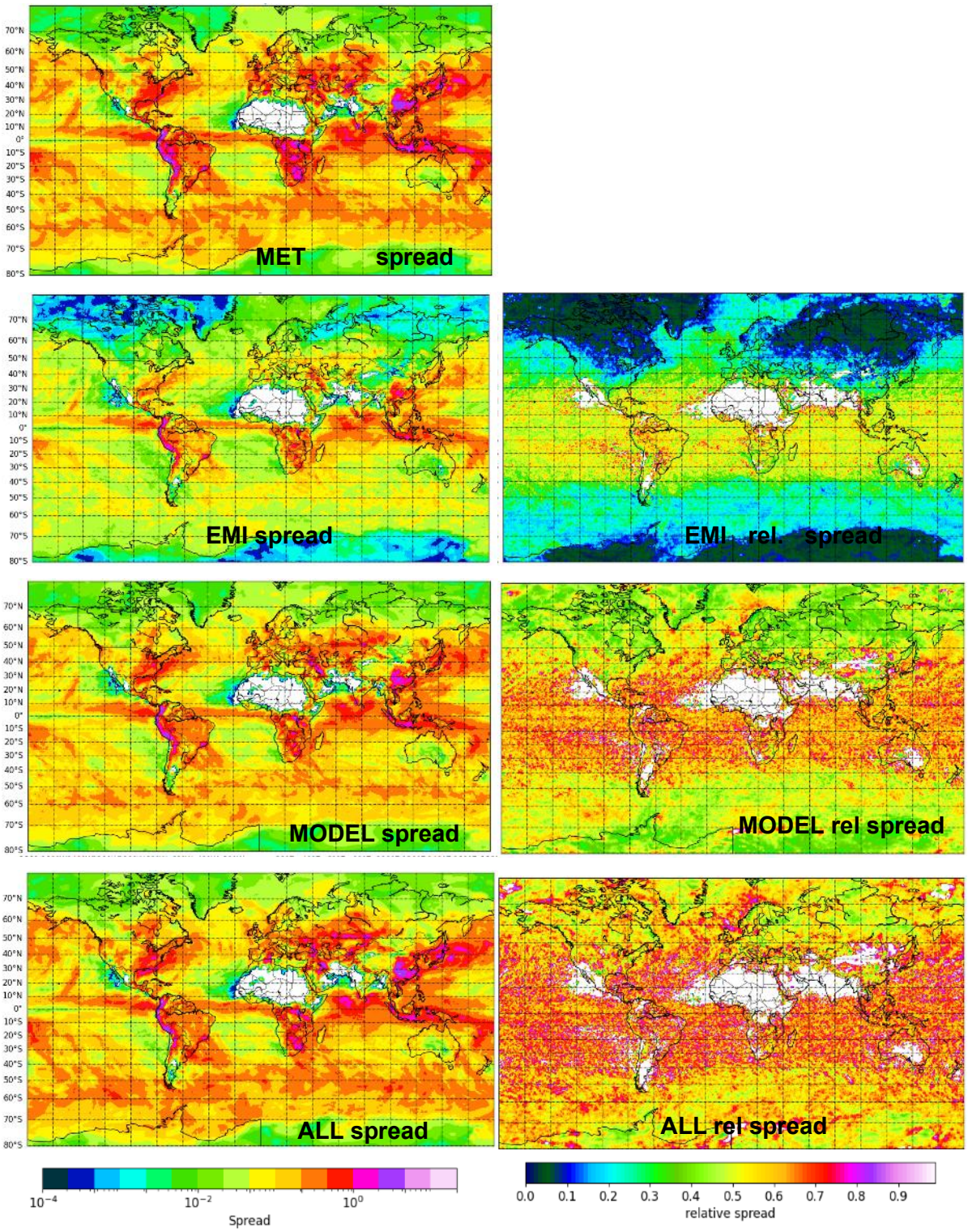

Figure 24: Spread (left) in g/m²/yr and relative spread (right) of the MET, EMI, MODEL and ALL experiments for simulated sulfate wet deposition in February 2021, at 24h forecast time.

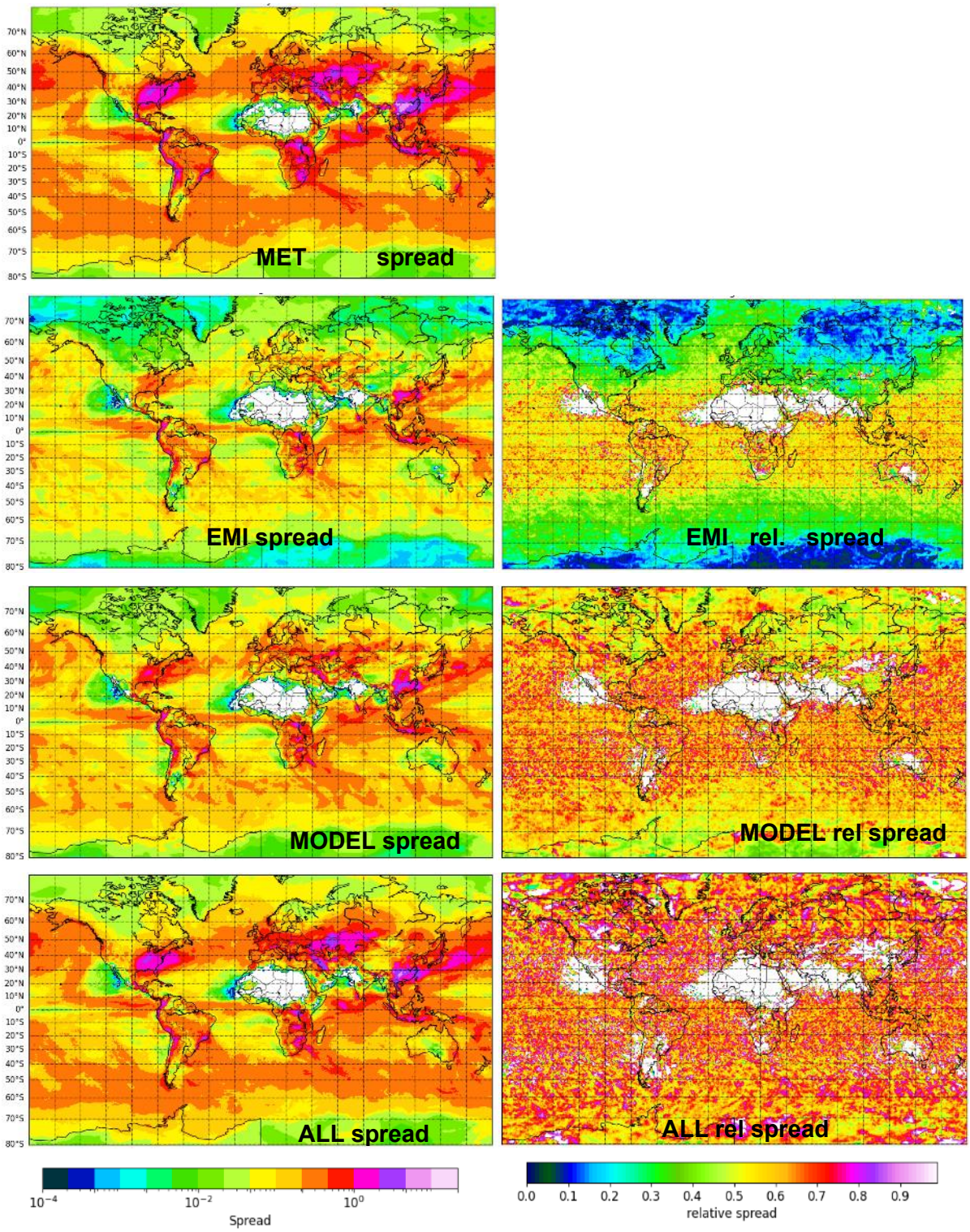

Figure 25: Spread (left) in g/m²/yr and relative spread (right) of the MET, EMI, MODEL and ALL experiments for simulated sulfate wet deposition in February 2021, at 120h forecast time.

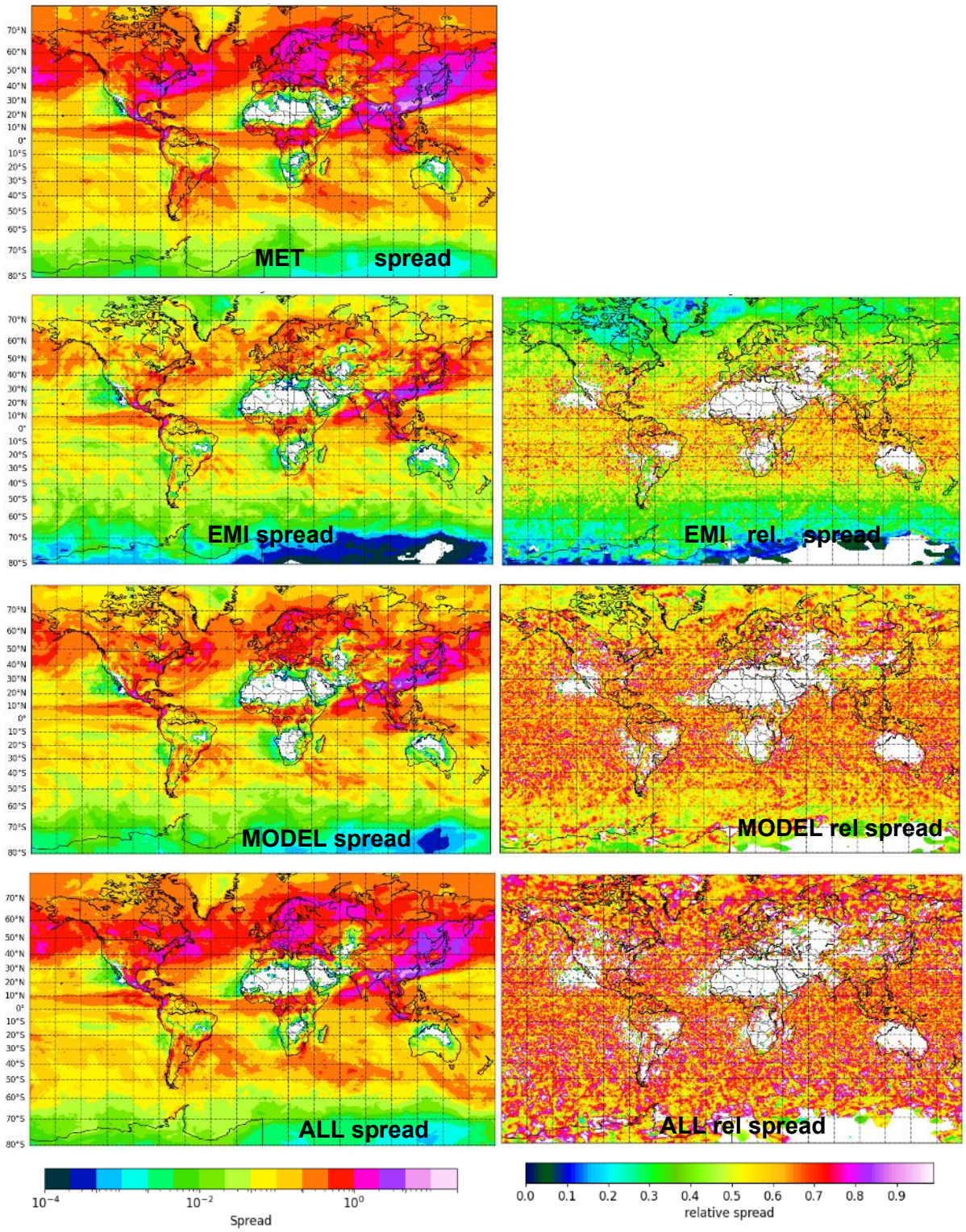

Figure 26: Spread (left) in g/m²/yr and relative spread (right) of the MET, EMI, MODEL and ALL experiments for simulated sulfate wet deposition in May 2021, at 120h forecast time.

6.3 Organic matter

6.3.1 Dry deposition

The absolute and relative uncertainty of organic matter dry deposition are shown in Figures 27, 28 and 29. Unlike sulfate, there are no oceanic sources of organic matter in IFS-COMPO, so the absolute spread values are generally higher over continents than over oceans, but this is not the case for relative spread. The absolute spread is much lower than that of sulfate, with maximum values over the main biomass burning and anthropogenic emission regions of 0.05 to 0.1 g/m²/year. The relative spread is also lower than for sulfate dry deposition over oceans for all experiments except ALL, with values between 10 and 25% for MET, 5% for EMI, 30% for MODEL. For ALL, the values reach 40 to 50% over most of oceans, and generally lower values (30-50%) over continental areas. The increase with forecast time is quite significant in general, particularly for EMI over continental areas. The differences between February and May 2021 mainly concern the different biomass burning areas, with in particular a large fire event in Central Siberia. Apart from that, the relative spread values are in the same range between the two months.

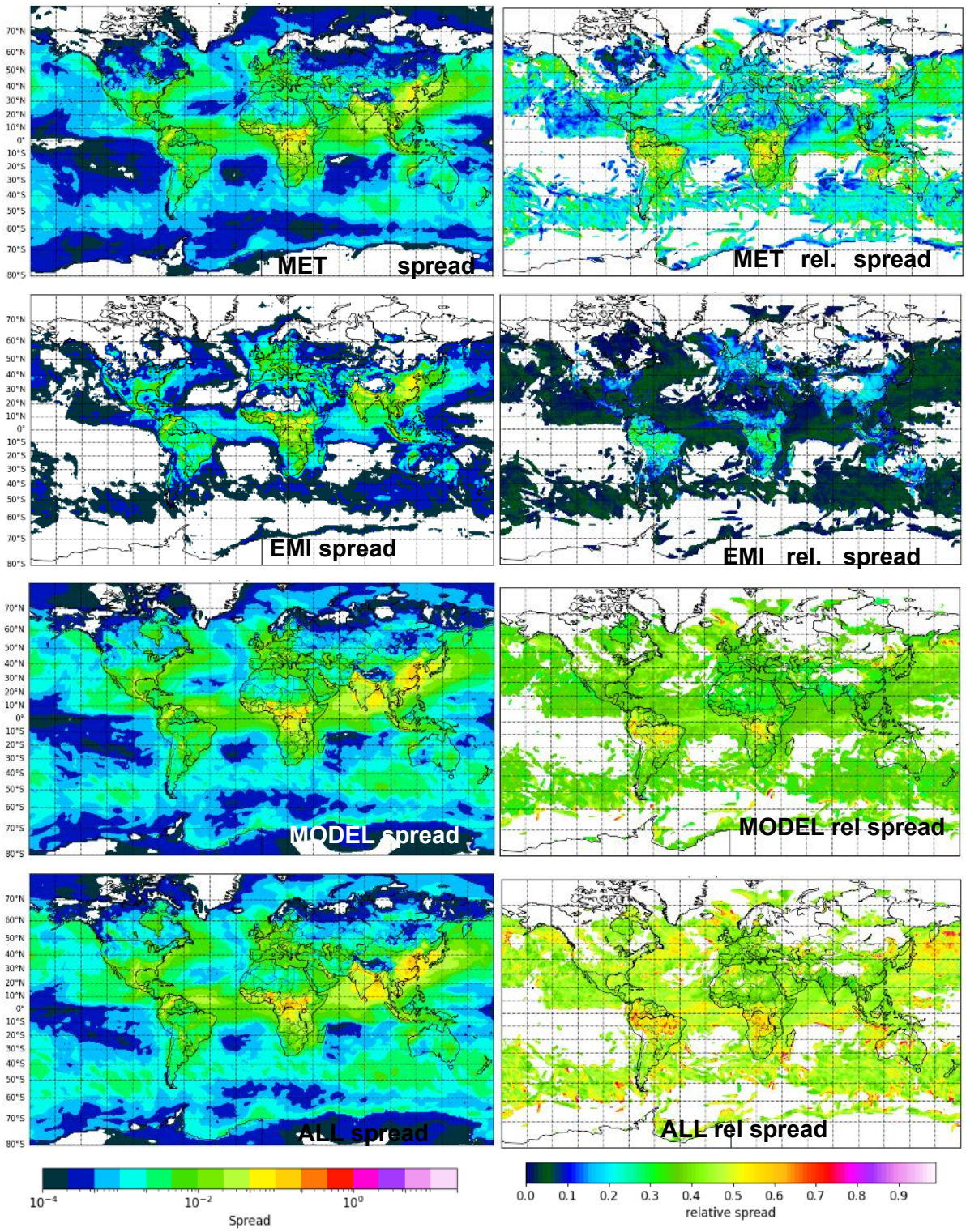

Figure 27: Spread (left) in g/m²/yr and relative spread (right) of the MET, EMI, MODEL and ALL experiments for simulated organic matter dry deposition in February 2021, at 24h forecast time.

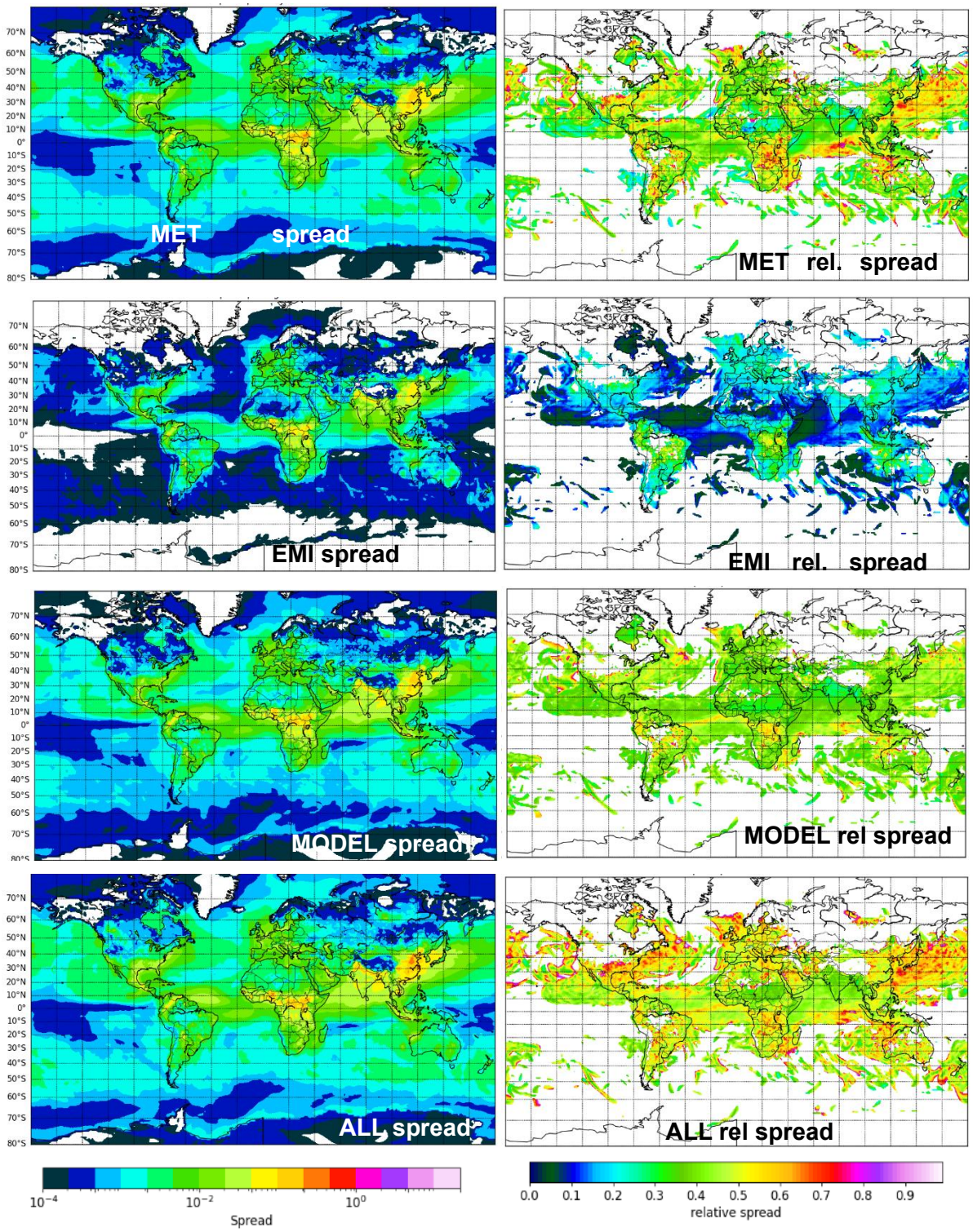

Figure 28: Spread (left) in g/m²/yr and relative spread (right) of the MET, EMI, MODEL and ALL experiments for simulated organic matter dry deposition in February 2021, at 120h forecast time.

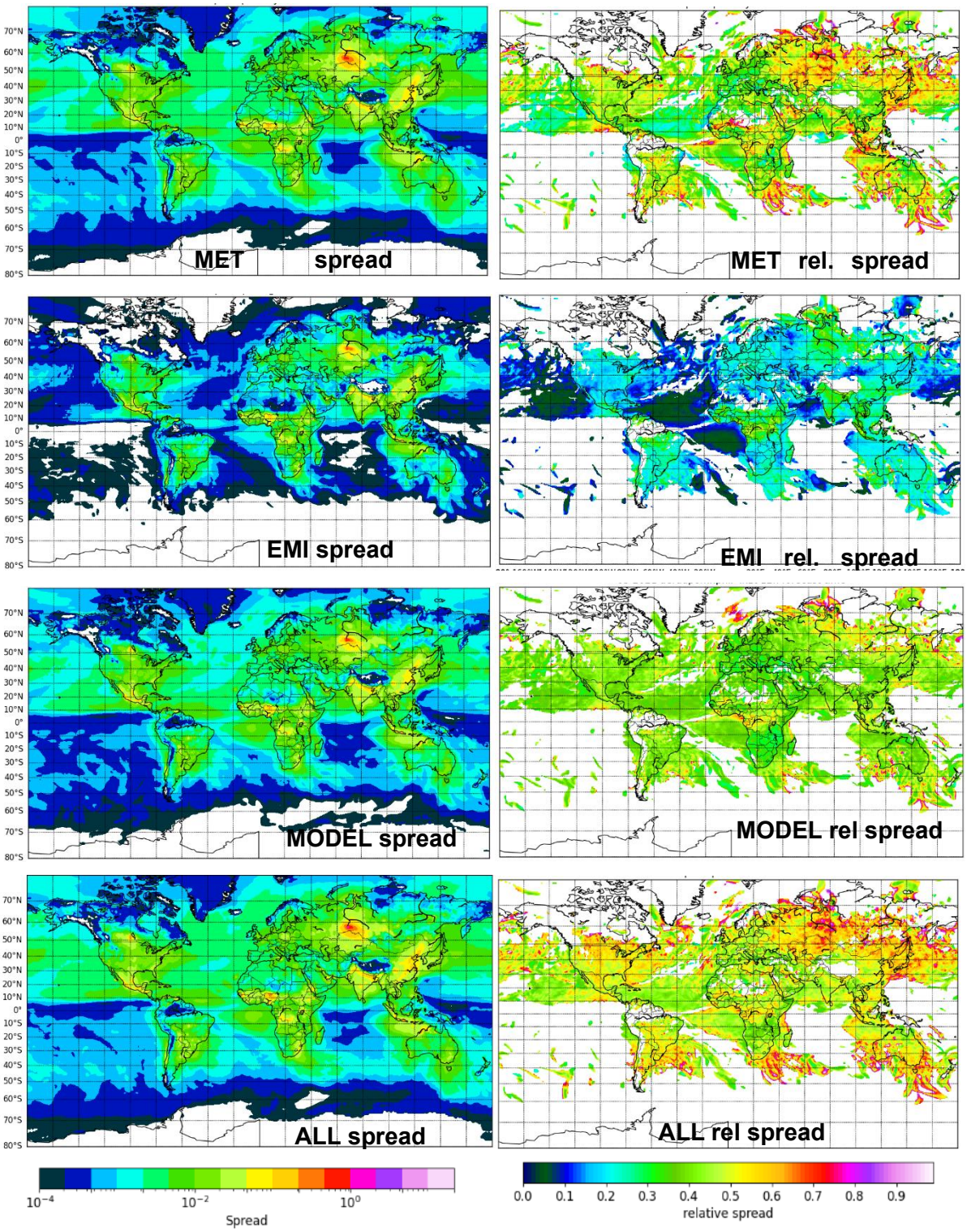

Figure 29: Spread (left) in g/m²/yr and relative spread (right) of the MET, EMI, MODEL and ALL experiments for simulated organic matter dry deposition in May 2021, at 120h forecast time.

6.3.2 Wet deposition

The absolute and relative uncertainty of organic wet deposition is shown in Figures 30, 31 and 32. As for sulfate, the values are much higher than for dry deposition, and the biomass burning regions (Central Africa and Amazon in February, Siberia in May) are much more prominent, which is because the relative contribution of biomass burning event to the simulated organic matter burden (which drives wet deposition, together with precipitation fluxes) is higher than to the simulated organic matter surface concentration (which drives dry deposition, together with wind) as a large fraction of biomass burning emissions are injected at heights well above the surface. The maximum absolute uncertainty reaches about 0.5 to 1 g/m²/year above Equatorial Africa. As for sulfate, the relative spread is very noisy, with values similar to that of sulfate wet deposition. The increase of the spread with forecast time is significant with EMI, but less so for the other experiments. As for sulfate wet deposition, the patterns show some evolution in May 2021 as compared to February 2021, following the evolving biomass burning patterns, but the relative spread, very noisy, shows values in the same range.

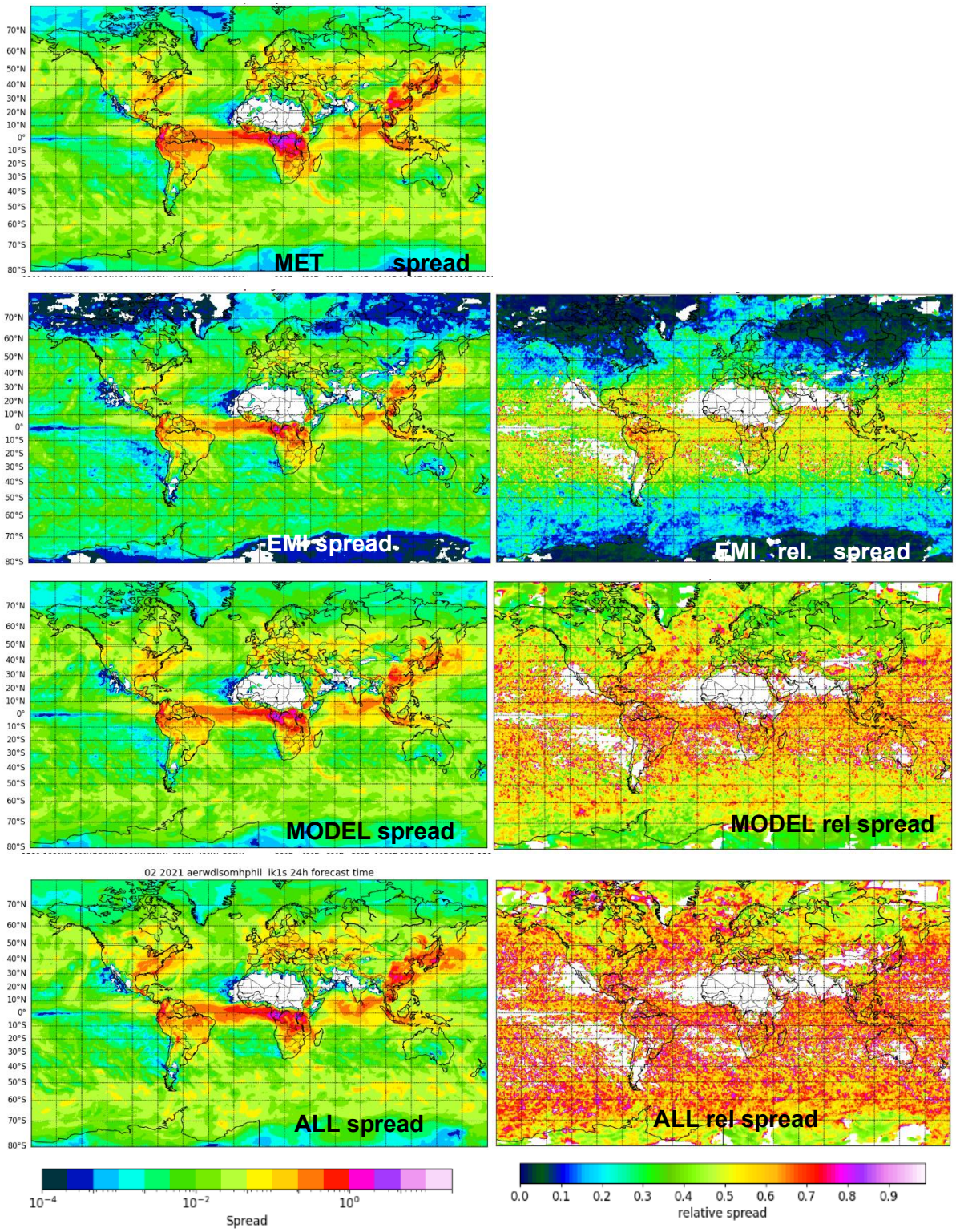

Figure 30: Spread (left) in g/m²/yr and relative spread (right) of the MET, DUST, MODEL and ALL experiments for simulated organic matter wet deposition in February 2021, at 24h forecast time.

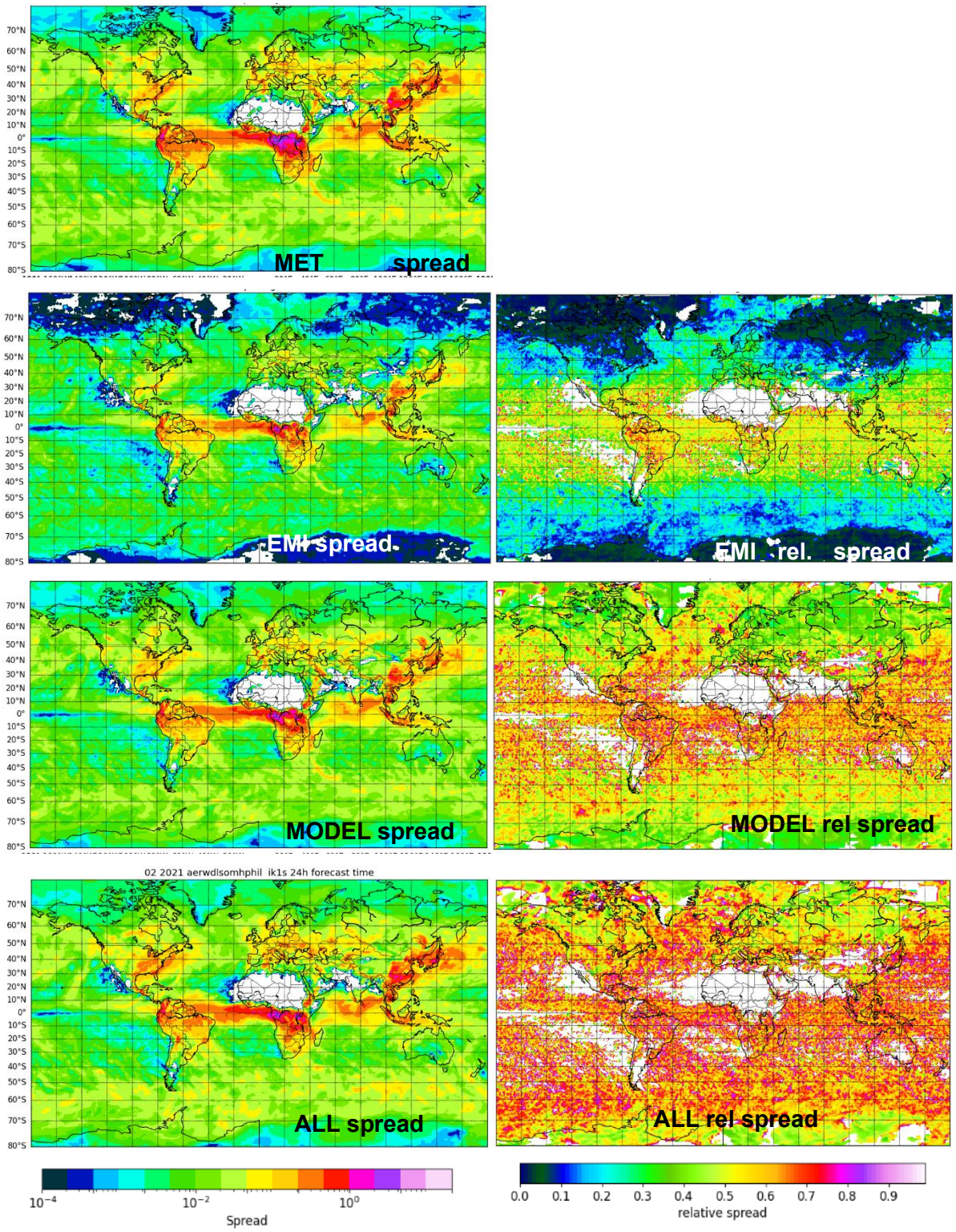

Figure 31: Spread (left) in g/m²/yr and relative spread (right) of the MET, DUST, MODEL and ALL experiments for simulated organic matter wet deposition in February 2021, at 120h forecast time.

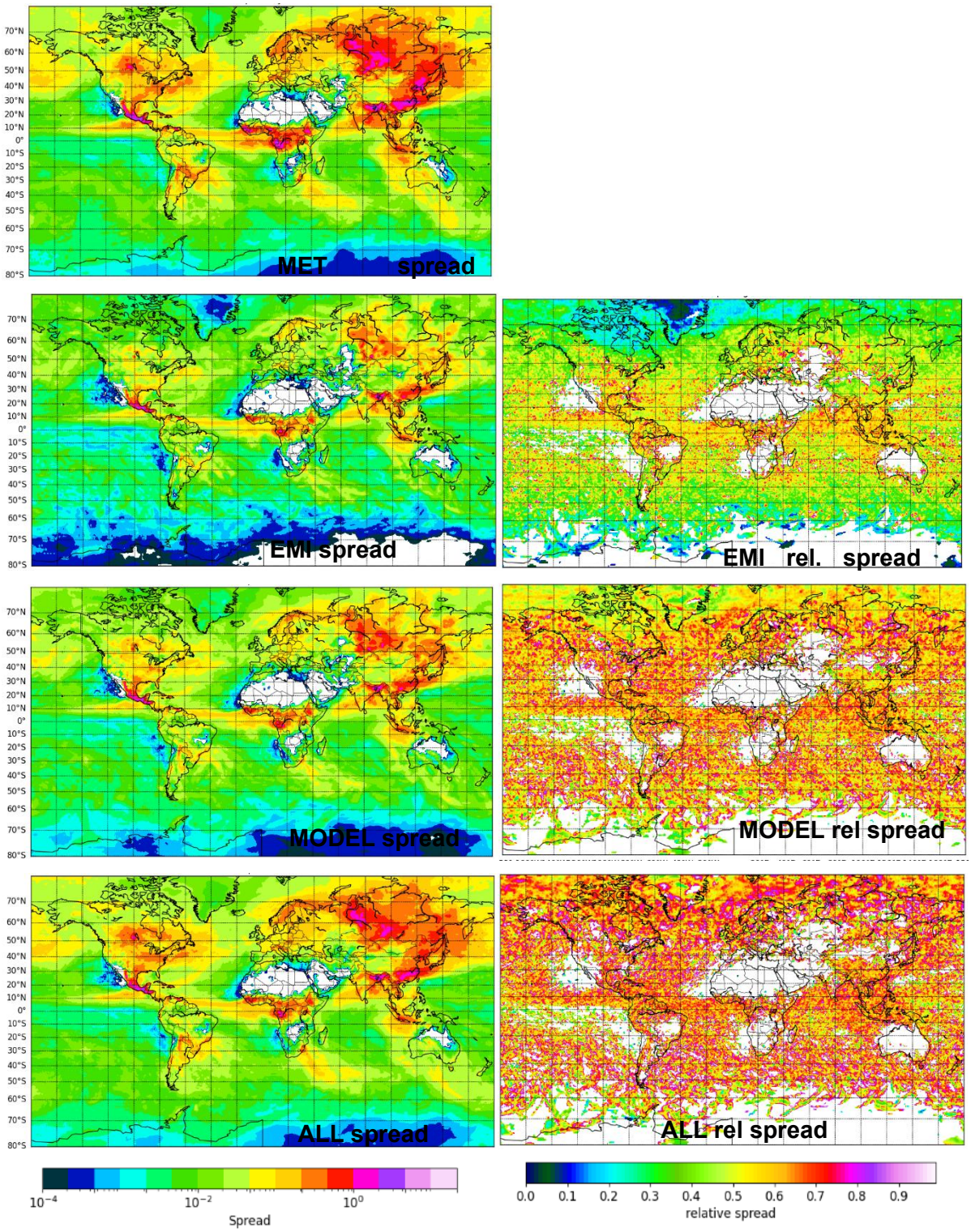

Figure 32: Spread (left) in g/m²/yr and relative spread (right) of the MET, DUST, MODEL and ALL experiments for simulated organic matter wet deposition in May 2021, at 120h forecast time.

6.4 Nitric acid wet deposition

Finally, Figures 33 and 34 show the absolute and relative spread of the nitric acid wet deposition fluxes at 24h forecast time, in February and May 2021. Source regions are quite prominent for the absolute spread for all experiments, with values between 0.2 and 1 kg/m²/day over the main anthopogenic emissions regions, but the outflow concerns most of oceans with non negligible values as well, modulated by the occurrence of precipitations. The relative spread values of MET (20-35% over oceans) are higher than thos of EMI (5-20%), but lower than that of MODEL (30-50% over oceans) and ALL. There is a clear anti correlation between absolute and relative spread, with very high values of relative spread where the absolute spread is low, showing that those high values are an artifact created by low values of the denominator in the normalisation operation.

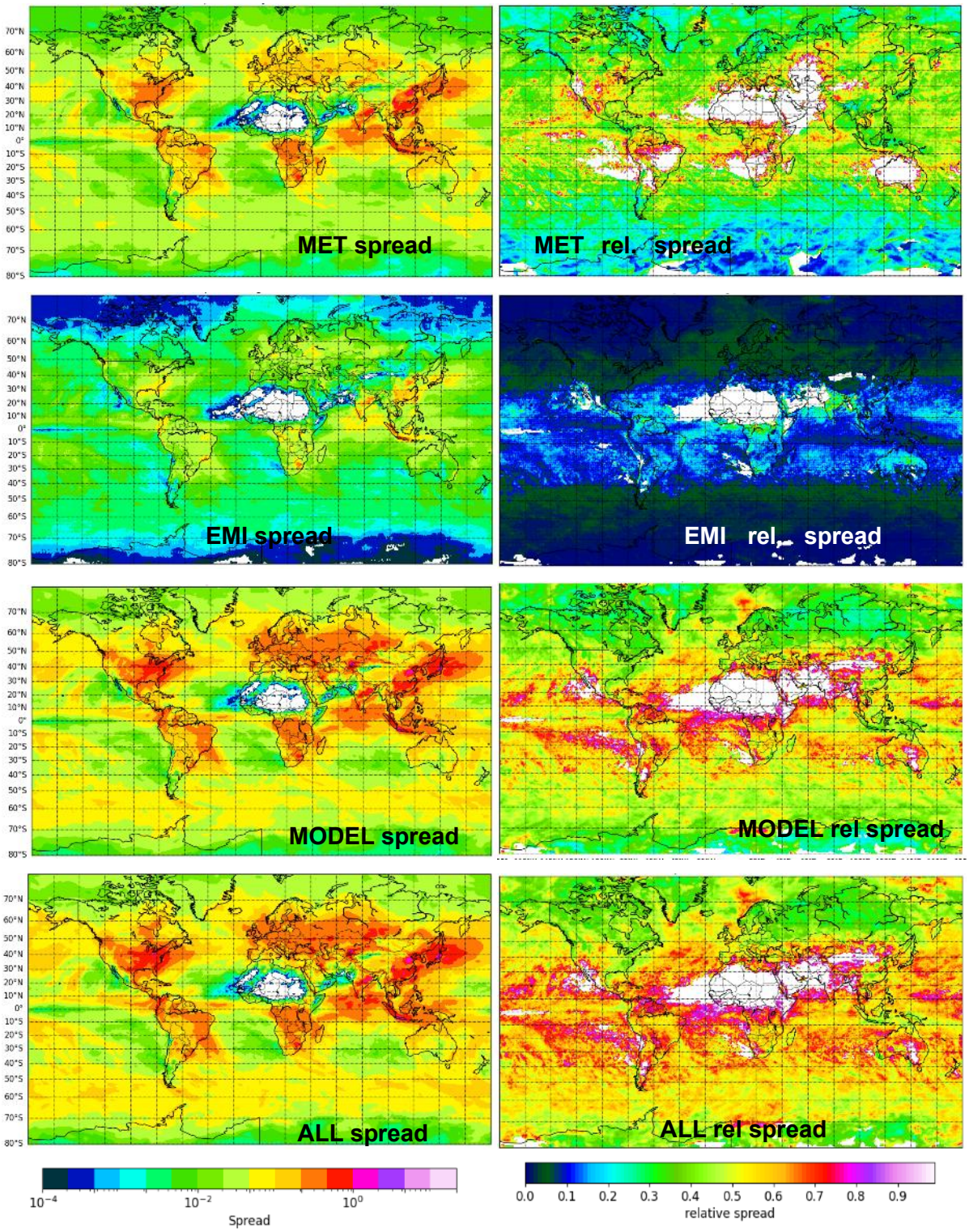

Figure 33: Spread (left) in kg/m²/day and relative spread (right) of the MET, EMI, MODEL and ALL experiments for simulated nitric acid wet deposition in February 2021, at 24h forecast time.

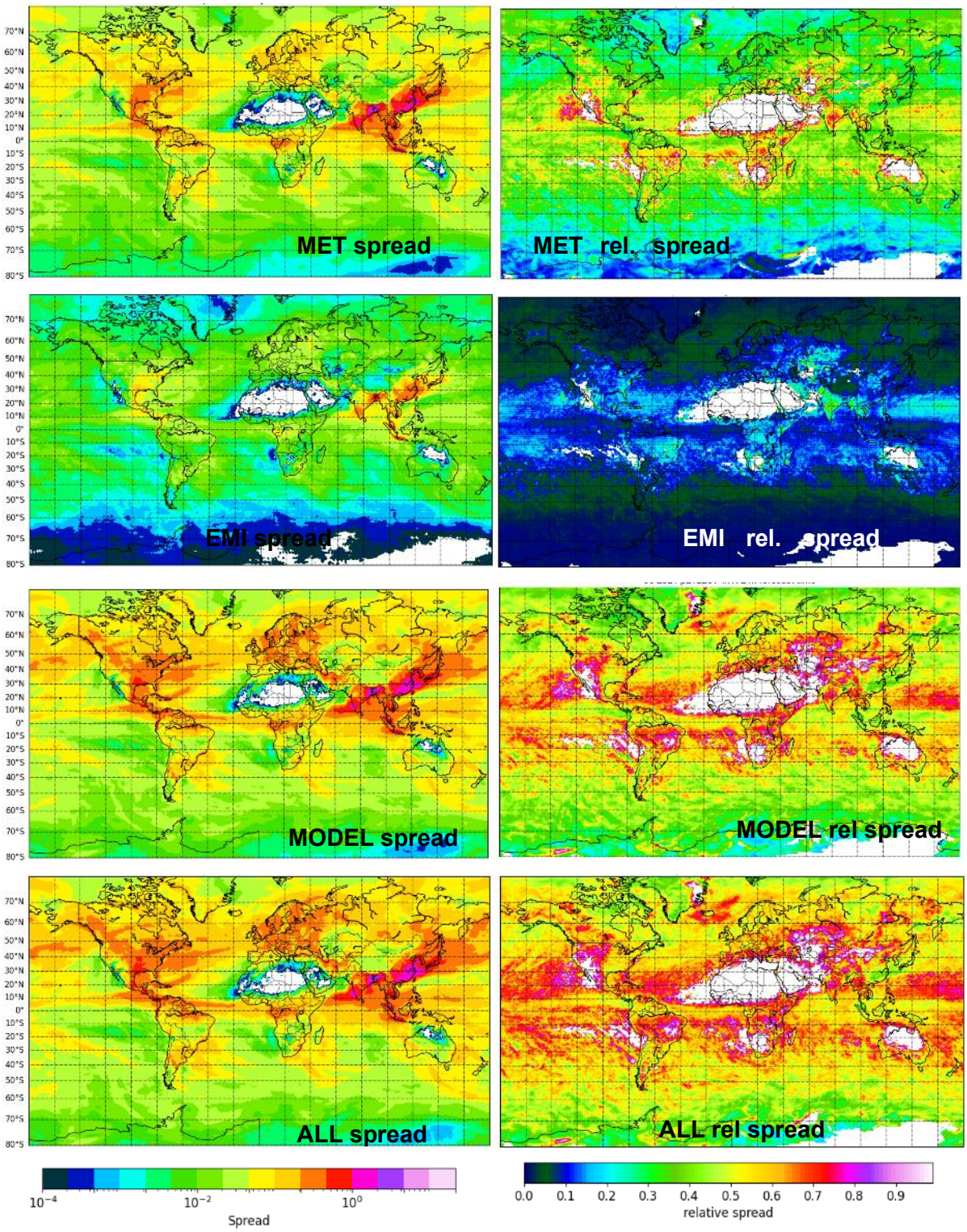

Figure 34: Spread (left) in kg/m²/day and relative spread (right) of the MET, EMI, MODEL and ALL experiments for simulated nitric acid wet deposition in May 2021, at 24h forecast time.

7 Conclusion

In this report we showed quantitative estimates of the uncertainties of a selection of CAMS global deposition products with a cycle close to that of the current global operational cycle 49R1, valid for 2021, which can give a qualitative assessment of uncertainties outside of 2021. The uncertainties vary a lot between species, forecast time, and the type of perturbations applied. The results also differ markedly between dry and wet deposition.

All sources of error combined, the uncertainty of most of dry deposition products at 24h forecasts is often in the range of 20-40%. Emissions in general bring relatively less uncertainty than model and meteorological errors. This could also arise from the choice of perturbations applied to emissions. The uncertainty resulting from the combination of all factors (meteorology, emissions, model error) is much lower than the sum of the uncertainty of each of these factors taken independently. It also means that the uncertainty from a combination of factors cannot be derived from the uncertainties of each factor taken separately. This work also helps in understanding the sensitivity of the simulated deposition to the different inputs of the deposition parameterizations.

These results were obtained with a first prototype of an IFS-COMPO ensemble. Diagnostics were developed to assess the skill of the ensemble as compared to observations and showed that all our ensemble simulations are under-dispersive: they fail to capture the whole variability of the observations, partly because of systematic model biases. This means that improving the skill of the model (debiasing, but also adding more degree of freedoms so as to better represent extremes) would allow for a lower uncertainty in the sense that fewer and or smaller perturbations would be needed to capture the observational variability More work is needed in order to derive perturbations that have more impact; inspiration could be drawn from the meteorological ensemble and the singular vector approach could be used for atmospheric composition perturbations.

8 References

Slingo Julia and Palmer Tim, 2011: Uncertainty in weather and climate prediction Phil. Trans. R. Soc. A.3694751–4767 http://doi.org/10.1098/rsta.2011.0161. Accessible at https://royalsocietypublishing.org/doi/epdf/10.1098/rsta.2011.0161

Holland, E. A., Braswell, B. H., Lamarque, J.-F., et al.: Variations in the predicted spatial distribution of atmospheric nitrogen deposition and their impact on carbon uptake by terrestrial ecosystems, J. Geophys. Res., 102, 15 849–15 866, 1997.

Lamarque, J. F., Kiehl, J. T., Brasseur, G. P., et al.: Assessing future nitrogen deposition and carbon cycle feedback using a multimodel approach: Analysis of nitrogen deposition, J. Geophys. Res., 110, 1–21, doi:10.1029/2005JD005825, 2005.

Luo, G., Yu, F., and Schwab, J.: Revised treatment of wet scavenging processes dramatically improves GEOS-Chem 12.0.0 simulations of surface nitric acid, nitrate, and ammonium over the United States, Geosci. Model Dev., 12, 3439–3447, https://doi.org/10.5194/gmd-12-3439-2019, 2019.

Reay, D. S., Dentener, F., Smith, P., Grace, J., and Feely, R. A.: Global nitrogen deposition and carbon sinks, Nat. Geosci., 1, 430–437, 2008.

Tan, J., Fu, J. S., Dentener, F., Sun, J., Emmons, L., Tilmes, S., Sudo, K., Flemming, J., Jonson, J. E., Gravel, S., Bian, H., Davila, Y., Henze, D. K., Lund, M. T., Kucsera, T., Takemura, T., and Keating, T.: Multi-model study of HTAP II on sulfur and nitrogen deposition, Atmos. Chem. Phys., 18, 6847–6866, https://doi.org/10.5194/acp-18-6847-2018, 2018.

Shephard, M. W., Dammers, E., Cady-Pereira, K. E., Kharol, S. K., Thompson, J., Gainariu-Matz, Y., Zhang, J., McLinden, C. A., Kovachik, A., Moran, M., Bittman, S., Sioris, C. E., Griffin, D., Alvarado, M. J., Lonsdale, C., Savic-Jovcic, V., and Zheng, Q.: Ammonia measurements from space with the Cross-track Infrared Sounder: characteristics and applications, Atmos. Chem. Phys., 20, 2277–2302, https://doi.org/10.5194/acp-20-2277-2020, 2020.

Sun, Y. *et al.* Negative effects of the simulated nitrogen deposition on plant phenolic metabolism: A meta-analysis. *Sci. Total Environ.* **19**, 137–142, 2020.

Wesely, M.: Parameterization of surface resistances to gaseous dry deposition in regional-scale numerical models. Atmospheric Environment (1967), 23(6), 1293–1304, doi:https://doi.org/10.1016/0004-6981(89)90153-4, 1989.

Zhang, L. and He, Z.: Technical Note: An empirical algorithm estimating dry deposition velocity of fine, coarse and giant particles, Atmos. Chem. Phys., 14, 3729–3737, https://doi.org/10.5194/acp-14-3729-2014, 2014.

Document History

Version	Author(s)	Date	Changes
1.0	Samuel Remy	16/09/2025	Initial version
1.1	Samuel Remy	28/09/2025	New version after reviews

Internal Review History

Internal Reviewers	Date	Comments
JF Müller (BIRA-IASB) and YM Drenan (Armines)	22/09/2025	Internal review